Onset of propagation of planar cracks in heterogeneous media

Sharad Ramanathan* and Daniel S. Fisher
Lyman Laboratory of Physics, Harvard University, Cambridge, Massachusetts 02138
(Received 16 December 1997)

The dynamics of planar crack fronts in hetergeneous media near the critical load for onset of crack motion are investigated both analytically and by numerical simulations. Elasticity of the solid leads to long-range stress transfer along the crack front which is nonmonotonic in time due to the elastic waves in the medium. In the quasistatic limit with instantaneous stress transfer, the crack front exhibits dynamic critical phenomenon, with a second-order-like transition from a pinned to a moving phase as the applied load is increased through a critical value. At criticality, the crack front is self-affine, with a roughness exponent $\zeta = 0.34 \pm 0.02$. The dynamic exponent z is found to be equal to 0.74 ± 0.03 and the correlation length exponent $\nu = 1.52 \pm 0.02$. These results are in good agreement with those obtained from an epsilon expansion. Sound-travel time delays in the stress transfer do not change the static exponents but the dynamic exponent z becomes exactly one. Real elastic waves, however, lead to overshoots in the stresses above their eventual static value when one part of the crack front moves forward. Simplified models of these stress overshoots are used to show that overshoots are relevant at the depinning transition leading to a decrease in the critical load and an apparent jump in the velocity of the crack front directly to a nonzero value. In finite systems, the velocity also shows hysteretic behavior as a function of the loading. These results suggest a first-order-like transition. Possible implications for real tensile cracks are discussed. [S0163-1829(98)05125-X]

I. INTRODUCTION

The dynamics of cracks in heterogeneous media is a very rich field involving much physics that is yet to be understood. Even in situations in which the *path* of a crack is predetermined—for example by a preweakend fault—its dynamics can still be complicated. The simplest situation is a crack confined to a plane. For small loads across such a planar crack, the crack front will be at rest. As the load is gradually increased, the crack front may undergo some transient motion but then again be arrested. If the load is increased above a critical load, however, the crack front will begin to propagate through the sample. The behavior near to the *onset* of propagation of planar cracks—in particular tensile cracks—is the subject of this paper.

In recent years there has been considerable theoretical progress towards understanding the dynamics of elastic manifolds moving through random media, such as charge-density waves,[3] fluid-surface contact lines,[4] and interfaces between two phases.[1,2] All of these exhibit a type of nonequilibrium critical phenomenon near to the onset of motion. However there are various features which make the system of a planar crackfront moving through a heterogeneous medium different from these other systems.

For cracks (as well as for contact lines) the bulk degrees of freedom lead to effective long-range interactions between the points on the front.[7,6] Thus, when a point on the crack front moves ahead, the stress at all other points on the front increases due to the elastic interactions tending to pull them forward. In addition, elastic waves are emitted as the crack front moves nonuniformly. When one point moves ahead, these waves result in stresses elsewhere on the front which, for a while, are greater than those due to just the static elastic deformations which will obtain long after the waves have passed. Both these *stress overshoots* and the long range interactions have earlier been shown to play a crucial role in the dynamics of the crack front when it is moving with a nonzero mean velocity.[8,9]

In the *absence* of these stress overshoots—as obtained if the stress transfer is quasistatic—many aspects of the dynamics of a planar crack front near the onset of motion can be understood by analogy with interfaces, in particular via a functional renormalization-group analysis, which for cracks, as for contact lines, entails an expansion about two dimensions.[4] The phenomenology is built on the existence of two ''phases'' which are separated by a *unique* critical load. When the applied load G^{∞} is small, there is no steady-state motion and the crack front is pinned by the random toughness in one of many locally stable configurations—we will ignore here and henceforth the effects of thermal creep. As the load is increased adiabatically, there are a series of local instabilities of the crack front which lead to ''avalanches'' that can become large as G^{∞} is increased further. Eventually at the critical load G_c^{qs} the crack front depins and begins to move, albeit very jerkily, with a nonzero, mean steady-state velocity, v. In an infinite system, this transition from the stationary to the moving phase exhibits nonequilibrium dynamic critical phenomena somewhat analogous to those near conventional second-order transitions. One macroscopic manifestation of this is the behavior of the mean velocity of the crack front at a load just above the critical load:

$$v \sim (G^{\infty} - G_c^{qs})^{\beta}. \tag{1}$$

A natural question that arises is the role of the stress overshoots left out of the quasistatic analysis. In particular, what are their effects on the crack dynamics and how do these affect the depinning transition? The temporal shape of the stress overshoots seen by a point on the crack front depends on various microscopic details, such as the microscopic re-

sponse time of the crack front, acoustic damping processes, etc. How the dynamics of the crack front depends on the nature of the stress overshoots and if there is any limit in which the dynamics of the medium can be neglected are not understood; these are questions that must be addressed. In particular, in the presence of stress overshoots, is there a regime in which a second-order-like transition from the pinned to the moving state persists or does the crack front always jump directly to a finite velocity? If the stress overshoots are ''relevant'' at the depinning transition do they make the velocity versus loading curves hysteretic? In either case, is the ''moving phase'' just above the threshold a nontrivial statistically stationary state or is it characterized by noisy linear dynamics? Thus, there are a large number of unanswered questions even in the seemingly simple problem of the dynamics, near the threshold, of a crack front restricted to move in a plane.

In this paper we study the dynamics of a crack front restricted to move in a plane, through a three-dimensional solid with heterogeneities only in the local fracture toughness. The effects of both the long-range interactions and the stress pulses are considered, and some of the questions raised above addressed. In the absence of the stress overshoots, we obtain, numerically, some of the exponents which characterize the transition from the stationary to the moving phase, check the scaling laws that have been predicted and compare the exponents with the analytical results obtained earlier by the $2-\varepsilon$ expansion.[4] We then extend the analysis to include the effects of sound-travel time delays in the stress transfer. Finally, we treat the effects of the stress overshoots on the depinning transition. Both the dynamic stresses obtained from a scalar approximation to elasticity and sharp pulselike overshoots are studied.

A. Outline

Before introducing the basic model and summarizing our main results, we give an outline of the paper. In Sec. II, the details of the models and the numerical methods employed are described. Section III A contains the results of the quasistatic model, where the stress transfer is instantaneous, while Sec. III B contains those in the case where there are acoustic time delays in the stress transfer. In Sec. IV, the effects of various kinds of stress overshoots are explored. Finally the results and their possible implications are discussed in Sec. V. The ''no-passing rule''[10] for these models, which plays an essential role in the analytical results, is discussed in Appendix A. Appendix B has the detailed forms of the kernels used in the numerical simulations.

B. Summary of results

The equation of motion for the crack front can be obtained by requiring energy conservation at all points on the crack front. This implies that the elastic energy flux into the crack, which is a nonlocal functional in both space and time of the shape of the crack front as well as of the local velocity of the crack front, must be equal to the surface energy required to create the new crack surface, i.e., the *local fracture toughness*. The general *linearized* equation of motion for a crack front moving along the positive x direction has the form,

$$\partial_t f(z,t) = \int_{t'<t} dt' \mathcal{P} \int dz' J(z-z',t-t') \partial_{t'} f(z',t') - \gamma[f(z,t),z] + \mathcal{E}, \tag{2}$$

where z is the coordinate along the crack front, $\mathcal{P}$ denotes the principal part of the integral, $f(z,t)$ is the deviation of the crack front from a straight one, γ is a random variable associated with the random position dependent fracture toughness in the solid and $\mathcal{E}$ represents the driving ''force'' due to the applied load G^{∞}. The kernel J is nonlocal both in space and time. This nonlocality arises from the long-range elastic interactions and the sound waves which are emitted as the crack moves. Note that because the basic processes near threshold consist of sections of the front moving ahead and stopping—i.e., roughly step functions in time—we have chosen to write the stress transfer in terms of $\partial_{t'} f(z',t')$, so that these jumps are approximately δ functions in t'.

We will classify the models based on whether or not the kernel J is *monotonic* in time at every spatial coordinate z. Monotonicity of the stress transfer plays a crucial role. It means that as a segment of the crack moves forward, the stress at all other points increases monotonically in time. This *convexity* property yields stringent constraints on the behavior as shown in Appendix A. It implies that a configuration of the crack which is behind another configuration at one time will remain behind the other configuration at all later times. This immediately leads to the conclusion that there is a unique critical load G_c^{qs} for monotonic models.

1. Quastatic approximation

We first consider the quasistatic approximation in which sound waves are neglected and the stress transfer is *instantaneous* so that the kernel is naturally monotonic. In this case, the basic phenomenology is well known.[3,4,1] As the load G^{∞} is gradually increased, segments of the crack front will overcome the local toughness and jump forwards, perhaps causing other segments to jump and thereby triggering an avalanche which will eventually be stopped by tougher regions. We find that, similar to driven interfaces, etc.,[3,4,1] the avalanches show a power-law size distribution[5] up to a characteristic length ξ_- with larger avalanches being much rarer. The distribution of avalanche size—roughly the extent along the crack front of an avalanche—has the form

$$\text{Prob}(\text{size of avalanche} > l) \approx \frac{1}{l^{\kappa}} \hat{\rho}(l/\xi_-). \tag{3}$$

The cutoff length, ξ_-, defines the correlation length below threshold. As the threshold load G_c^{qs} is approached, the correlation length ξ_- diverges as

$$\xi_- \sim (G_c^{qs} - G^{\infty})^{-\nu_-}. \tag{4}$$

At the threshold, there is no characteristic length scale and the distribution of the avalanche sizes is a pure power law. From Eq. (3) and scaling relations between the exponents, we expect that the cumulative probability of the size of an avalanche being greater than l, as the load is swept slowly from zero to the critical load scales as

$$\int_0^{G_{c,qs}^{\infty}} dG^{\infty} \frac{1}{l^{\kappa}} \hat{\rho}(l/\xi_-) \sim \frac{1}{l}; \tag{5}$$

this is in agreement with the numerics within error bars.

As the load increases above the critical load, the crack front begins to move with a mean velocity, which the monotonicity implies is unique. The velocity scales as in Eq. (1), with the velocity exponent, determined from our numerical simulations,

$$\beta = 0.68 \pm 0.06. \tag{6}$$

All quoted error bars here and henceforth are one-σ errorbars from χ^2 fits. Just above G_c^{qs} the motion of the front is very jerky with fluctuations in the velocity correlated up to a distance ξ_+, which diverges as one approaches the threshold from above as $\xi^+ \sim (G^{\infty} - G_c^{qs})^{-\nu_+}$.

The exponents ν_+ and ν_- will be equal i.e., $\nu_+ = \nu_- = \nu$, if there is only one divergent length scale in the problem, as predicted by the renormalization (RG) analysis.[1,4] Assuming this two-sided scaling, we can obtain the correlation length exponent, via finite-size scaling, from the dependence of the variance of the critical load on the size of the system as

$$\nu = 1.52 \pm 0.02. \tag{7}$$

At threshold, the crack front is self-affine with correlations

$$\langle [f(z,t) - f(z+r,t)]^2 \rangle \sim r^{2\zeta}, \tag{8}$$

where $\langle\ \rangle$ denotes the average over the randomness. The roughness exponent ζ is found numerically to be

$$\zeta = 0.34 \pm 0.02, \tag{9}$$

in excellent agreement with the $2-\varepsilon$ expansion prediction $\zeta \approx 1/3$.

The dynamic exponent is found from the duration of avalanches as a function of size l; they typically last for

$$\tau_l \sim l^z \tag{10}$$

with

$$z = 0.74 \pm 0.03. \tag{11}$$

The exponent identities predicted from the scaling and RG analysis[3,4]

$$\beta = (z - \zeta)\nu, \tag{12}$$

$$\nu = \frac{1}{1-\zeta}, \tag{13}$$

are found to be satisfied, so that there are only *two independent exponents*, say ζ and z, characterizing the transition.

2. Effects of sound travel time

For a model with a monotonic kernel but with the stress transfer delayed by the sound travel time, we argue that the static exponents ν and ζ are *identical* to the corresponding quasistatic case. Also, for every manifestation of the randomness, the critical load for this model G_c^{td} is exactly equal to that in the quasistatic approximation, G_c^{qs}. However, the dynamic exponent for this model is predicted to be $z=1$ exactly. Since the exponent identities Eqs. (12) and (13) also hold for this model, we obtain $\beta = 1$, which is consistent with the numerical results.

3. Sound waves and stress overshoots

The inclusion of the effects of sound waves leads to nonmonotonic kernels. These result in the stress at points on an advancing crack front being nonmonotonic in time, which substantially changes the physics. We have considered two types of nonmonotonic kernels. The first arises from a scalar approximation to elasticity theory and the second is a simpler one characterized by sharp pulses superimposed on the time-delayed stress transfer. In both cases we find that the overshoots in the stress are *relevant* at the depinning transition, causing large avalanches to run away and changing the nature of the transition from the pinned to the moving phase.

The model with sharp pulses involves nonmonotonic kernels of the form

$$J_{\mathrm{sp}}(z,t;\alpha,\gamma) = \Theta(t-|z|)/\pi z^2 + \alpha\,\delta(t-|z|)/|z|^{\gamma}. \tag{14}$$

For $\alpha = 0$, there are no stress pulses and the model reduces to the sound travel-time-delayed model and hence $G_c(\alpha = 0, \gamma)$ is identical to the threshold force for the quasistatic model, G_c^{qs}. We find, both from analytic arguments and from the numerics, that for small positive α and fixed $\gamma \geqslant 1/2$, the threshold load, $G_c(\alpha,\gamma)$, decreases with increasing α as

$$\langle G_c^{qs} - G_c^{\infty}(\alpha,\gamma) \rangle \sim \alpha^2. \tag{15}$$

This behavior is controlled by the relevant eigenvalue for the overshoot perturbation at the quasistatic depinning fixed point.

In a scalar approximation to elasticity theory, the stress overshoots have long tails in time. In addition, the rough crack front will affect the propagation of the stress pulses due to the nonlinearities neglected in Eq. (2). We argue that the basic features found in the sharp stress pulse model still obtain, in particular that the stress overshoots are *relevant* and change the nature of the transition. Numerical results using an appropriate class of kernels support this conclusion.

For real elastodynamics appropriate to a tensile crack, the stress transfer kernel, for a fixed z, is found to be initially negative, when the longitudinal sound waves arrive, and then change sign when the Rayleigh waves arrive. The stress peaks due to the Raleigh waves are similar to those in the scalar elastic approximation and we believe that they will have similar effects in decreasing the critical load. However, the more complicated nature of the stress transfer suggests that the depinning transition of tensile cracks may involve essential additional physics. Some tentative ideas in this direction are discussed at the end of the paper.

With or without the additional complications of the full elastodynamic stress transfer, the nature of the transition between a static and a moving crack front in the presence of stress overshoots is not resolved by our numerical or analytical results. The simplest scenario, which appears to be supported by the numerics, is a ''first-order'' transition with hysteresis from a pinned phase to a state with nonzero ve-

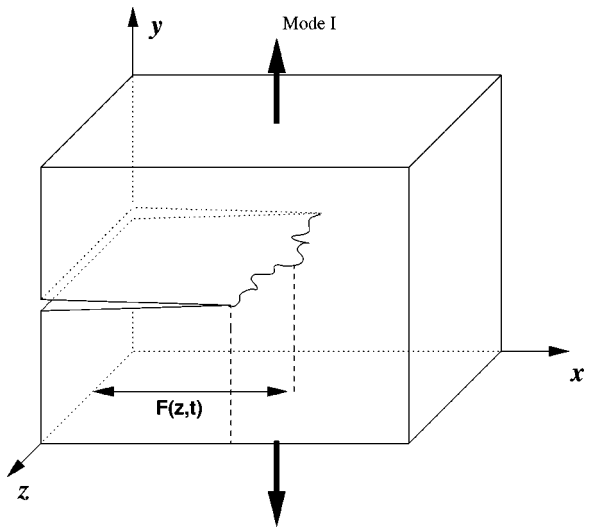

FIG. 1. Schematic of a planar crack propagating through a heterogeneous medium. The crack front $x=F(z,t)$ and the free crack surfaces, which are flat, are shown. The applied mode I (tensile) loading is also indicated.

locity. This may well be the correct scenario, but possible concerns and other possibilities are discussed in Sec. V.

II. MODELS

In this section we discuss the equation of motion for a real tensile crack and various approximations to it that we will study.

A. Geometry and equation of motion

We denote the plane in which the crack is confined $y=0$, with the crack open in the region $x<F(z,t)$. We assume that $F(z,t)$ is a single-valued function of z so that, the curve $x=F(z,t)$ describes the location of the crack front. Since the crack is planar, the fracture surfaces that it leaves behind are, of course, smooth. The geometry is shown in Fig. 1.

The vectorial displacement field $\vec{u}$, satisfies the equations of elastodynamics

$$\rho\partial_t^2 u_i=\partial_j\sigma_{ij} \tag{16}$$

with σ_{ij} the stress tensor. The displacement field, $\vec{u}(x,y=0^{\pm},z)$, has a discontinuity across the crack surface while the normal stresses, $\sigma_{iy}(y=0^{\pm})$, must vanish on the crack surface. For a crack with purely *tensile loading*, only u_y will be discontinuous and will have a $\sqrt{F(z,t)-x}$ singularity at the crack front with an amplitude proportional to the local mode I stress intensity factor, $K_I(z,t)$.[11] As long as the crack remains planar, symmetry under $y\rightarrow -y$ implies that the loading is purely mode I, so that we will simply use $K\equiv K_I$.[13] We consider the system under a static load applied far away so that for a straight crack at rest [i.e., $F(z,t)=\text{const}$], $K=K^{\infty}=\text{const}$.

As the crack front advances, $F\rightarrow F+\delta F$, an energy per unit area of the new crack surfaces exposed, $\Gamma[x=F(z,t),z]$, must be provided to the crack front in order to fracture the solid; in an ideal quasiequilibrium situation this is just twice the solid-vacuum interfacial energy density, more generally it is the local fracture toughness that includes the effects of small scale physics for which linear continuum elasticity is not valid. The fracture energy will be provided to the crack front by a flux of stored elastic energy per unit area of the new crack surface, $\mathcal{G}(z,t,\{F\})$, which in general depends on the past history of the whole crack front as well as its instantaneous local velocity $\partial F/\partial t$. The equation of motion of the crack front is obtained by requiring that the elastic energy released be equal to the surface energy required for fracture, i.e.,

$$\mathcal{G}[z,t,\{F(t'\leqslant t)\}]=\Gamma[x=F(z,t),z] \tag{17}$$

for all z and t. The available energy $\mathcal{G}$ has the general form

$$\mathcal{G}=A[v_{\perp}(z,t)]G[z,t\{F(t'<t)\}], \tag{18}$$

where $v_{\perp}$ is the local velocity normal to the crack front and G, which is independent of $\partial F/\partial t(z,t)$, is the elastic energy that would be released at (z,t) if the crack had advanced *adiabatically* at that point, i.e., with $\partial F/\partial t(z,t)=0$.[12]

For a straight stationary crack, $F=\text{const}$,

$$G=G^{\infty}=\frac{1-\nu^2}{E}(K^{\infty})^2, \tag{19}$$

with E the Young's modulus and ν the Poisson ratio.[14] When the crack advances at a nonzero velocity, not all of the released elastic energy is available for fracture; some fraction of it goes into the kinetic energy of the moving material very close to the front. The fraction of G available for fracture $A[v_{\perp}(z,t)]$ depends *only* on the local normal velocity; it decreases from unity for small $v_{\perp}$ and goes to zero for $v_{\perp}=c$, the Raleigh wave velocity. For a straight crack in a system with uniform toughness Γ this leads to a monotonic

$$v(G^{\infty})=A^{-1}(G^{\infty}/\Gamma) \tag{20}$$

for G^{∞} greater than the Griffith threshold, i.e., $G^{\infty}>\Gamma$. When G^{∞} is smaller than the Griffith threshold we assume that the crack does not move, i.e., once the solid breaks, the crack does not to reheal (this is in fact observed in most situations, with the absence of rehealing due to plastic and other irreversible deformations at the crack tip). The velocity of the crack is thus constrained to be positive.[15]

We are interested in the behavior near the depinning transition at which the crack starts to advance. We will use Eq. (17) as the starting point of our analysis of the dynamics of the crack front at this transition. The fracture toughness Γ in a *heterogeneous solid*, is a position-dependent quantity, which we write as

$$\Gamma(x,z)=\Gamma_0[1+\gamma(x,z)]$$

with Γ_0 the mean value of the fracture toughness and $\Gamma_0\gamma(x,z)$ the variable part of the fracture toughness which we will take to have a zero mean and covariance given by

$$\langle\gamma(x,z)\gamma(x',z')\rangle=\Upsilon(x-x',z-z') \tag{21}$$

with a function Υ which is, generally, short ranged in space.

The available energy $\mathcal{G}$ is a complicated nonlinear functional of the crack shape. In order to make progress, we will expand the position of the crack front in powers of the de-

viation, $f(z,t)$, away from a straight crack. The position of the crack front can be written as

$$F(z,t)=F_I+f(z,t), \tag{22}$$

where F_I is the original length of the crack which is assumed to be much larger than the scales of motion of the crack front so that the applied stress intensity factor K^∞ does not increase significantly as the crack advances. Thus, the stored elastic energy available to the crack front can thus be written in the form

$$\mathcal{G}=G^\infty[1+g(z,t,\{f\})],$$

where G^∞ is that for a straight crack of length F_I for the given external load. If $\partial f/\partial z$ is small, so will be g. To linear order in f, g can be written as

$$g=-P\otimes f,$$

where P is a kernel and $\otimes$ represents a convolution in space and time. For a tensile crack, the Fourier transform of P is[13,16]

$$P(k,\omega)=\left\{2\sqrt{k^2-\omega^2/c^2}-\sqrt{k^2-\omega^2/a^2}+\frac{1}{2\pi i}\oint dW\tilde{I}(W,k^2,\omega^2)\right\} \tag{23}$$

with

$$\tilde{I}=\frac{-\omega^2}{\sqrt{Wk^2-\omega^2}W^{3/2}}\ln\left[\left(2-\frac{W}{b^2}\right)^2-4\sqrt{1-\frac{W}{a^2}}\sqrt{1-\frac{W}{b^2}}\right]; \tag{24}$$

the contour integral circling in the counterclockwise direction the cut in the complex W plane that runs from $W=b^2$ to $W=a^2$ with a and b the longitudinal and transverse sound velocities, respectively; the argument of the logarithm in Eq. (24) the function whose zero W_0 determines the Raleigh wave velocity via $W_0=c^2$; and $\omega\to\omega+i0$ needed to define all cuts, e.g.,

$$\sqrt{k^2-\omega^2/c^2}=-i\ \mathrm{sgn}(\omega)\left|\sqrt{\omega^2/c^2-k^2}\right| \tag{25}$$

for $\omega^2\geqslant c^2k^2$. Thus,

$$P(k=0,\omega)=-i\omega B, \tag{26}$$

where B is a positive number.

To linear order in f, the equation of motion can be written as

$$P\otimes f=-\gamma(z,t)+\mathcal{E} \tag{27}$$

with the constraint that the local velocity of the crack front be positive and

$$\mathcal{E}=\frac{G^\infty-\Gamma_0}{G^\infty}, \tag{28}$$

which acts like the applied driving force on the crack front. From the general structure of the energy release $\mathcal{G}$ from Eq. (18), we can separate the kernel P into sum of two terms, one which just depends only on the local velocity of the crack front and the other which depends nonlocally on the shape of the crack front at all prior times. Thus, we can express P as

$$P(k,\omega)=-i\omega B+|k|\tilde{P}(\omega/|k|), \tag{29}$$

where $|k|\tilde{P}(\omega/|k|)$ is the nonlocal part which vanishes as $\omega\to\infty$. The equation of motion can then be written in the form

$$\begin{aligned}B\partial_t f=&\left\{\mathcal{P}\int_{z',t'<t}J(z-z',t-t')\partial_{t'}f(z',t')-\gamma(z,t)+\mathcal{E}\right\}\\&\times\Theta\left[\mathcal{P}\int_{z',t'<t}J(z-z',t-t')\right.\\&\left.\times\partial_{t'}f(z',t')-\gamma(z,t)+\mathcal{E}\right],\end{aligned} \tag{30}$$

where

$$J(z,t)=\int\int e^{ikz-i\omega t}\left[-\frac{|k|}{i\omega}\tilde{P}(\omega/|k|)\right] \tag{31}$$

and $\mathcal{P}$ denotes the principal part of the z integral. The Heaviside step function Θ constrains the velocity of the crack front to be positive and will not be written out explicitly henceforth.

The kernel J is readily evaluated from Eq. (23) to be

$$\begin{aligned}J(z,t)=&-\frac{at\Theta(at-|z|)}{\pi z^2(a^2t^2-z^2)^{1/2}}+\frac{2ct\Theta(ct-|z|)}{\pi z^2(c^2t^2-z^2)^{1/2}}\\&+\frac{1}{2\pi^2 i}\oint\frac{t}{\sqrt{W}(Wt^2-z^2)^{3/2}}\\&\times\ln\left[\left(2-\frac{W}{b^2}\right)^2-4\sqrt{1-\frac{W}{a^2}}\sqrt{1-\frac{W}{b^2}}\right],\end{aligned} \tag{32}$$

where the branch cuts are defined as previously.

The stress transfer kernel Eq. (32) is rather complicated. It is plotted as a function of t for a fixed z in Fig. 2 for a Poission's ratio, $\nu=0.25$. At the arrival time of the Raleigh waves, J diverges as $1/(ct-z)^{1/2}$ and then decays slowly to its long-time value, i.e., $J(z,t\to\infty)\to 1/\pi z^2$, the static stress transfer kernel. Although the negative stress precursor to the stress peak that occurs for $z/a<t<z/c$ may well be important, for our primary purposes here, we believe that the stress peak is the more important feature. It is therefore useful to study a somewhat simpler model which has a similar stress peak.

We choose to study a *scalar approximation* to elasticity theory. In this approximation the displacement field in the solid is take to be a scalar field ϕ, satisfying the three-dimensional scalar wave equation

$$\frac{1}{c^2}\partial_t^2\varphi-\nabla^2\varphi=0. \tag{33}$$

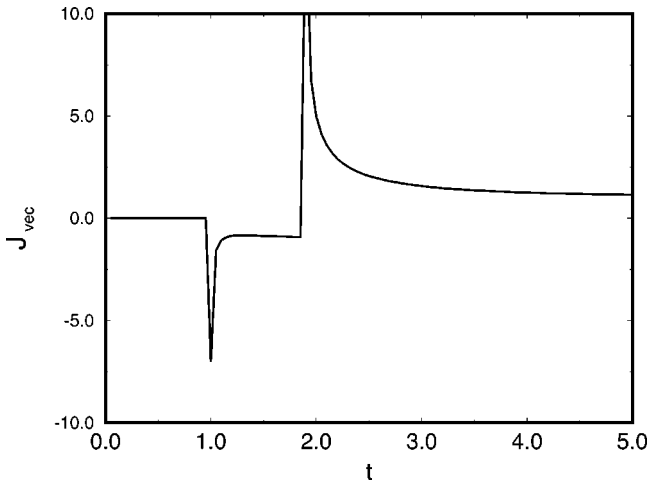

FIG. 2. Stress transfer kernel for a tensile crack is shown as a function of t at fixed distance $z=1$. The longitudinal sound velocity is set equal to one and the Poisson ratio chosen to be $\nu=0.25$. The stress pulse is initially negative and then changes sign. The divergences at times corresponding to the longitudinal and Rayleigh wave arrival times have been cut off.

The displacement field φ has a discontinuity across the crack surface while the normal derivative $\partial_y\varphi(y=0^{\pm})$ (the ''stress'') vanishes on the crack surface. We shall refer to this model as the *scalar model*. Under the external load, the displacement field φ has a $\sqrt{F(z,t)-x}$ singularity at the crack front proportional to the scalar stress intensity factor $K(z,t)$ as for real elasticity. The corresponding kernel P can be written in Fourier space as[8]

$$P_{\text{scalar}}=\sqrt{k^2-\omega^2/c^2} \tag{34}$$

and the stress transfer kernel is

$$J_{\text{se}}(z,t)=\frac{ct\Theta(ct-|z|)}{\pi z^2(c^2t^2-z^2)^{1/2}}. \tag{35}$$

We see that the stress peak, the long-time tail and the static stress transfer kernel $J(z,t\to\infty)$ are all of similar form to the real tensile crack case.

From the kernels Eqs. (32) and (35) we see that for both the tensile crack and the scalar model, sound waves yield nonmonotonic kernels which lead, in response to a jump of one segment of the crack front, to ephemeral overshoots of the stress above the eventual static value. The magnitude of the overshoots will be governed by microscopic factors such as the microscopic response time of the crack front and acoustic damping processes which can be incorporated by the replacement of ω^2 by $\Omega^2=\omega^2/(1-i\omega\tau_d)$ in Eq. (23) or Eq. (34) with τ_d an acoustic relaxation time. We are interested in how these overshoots affect the dynamics of the crack front near threshold. But in the limit that all crack disturbances move along the crack slowly compared to c, we can neglect the effects of sound waves, and the transfer of stress will be effectively instantaneous yielding the quasistatic model with the kernel given by[6]

$$J_{\text{qs}}(z,t)=\frac{1}{\pi z^2}\Theta(t). \tag{36}$$

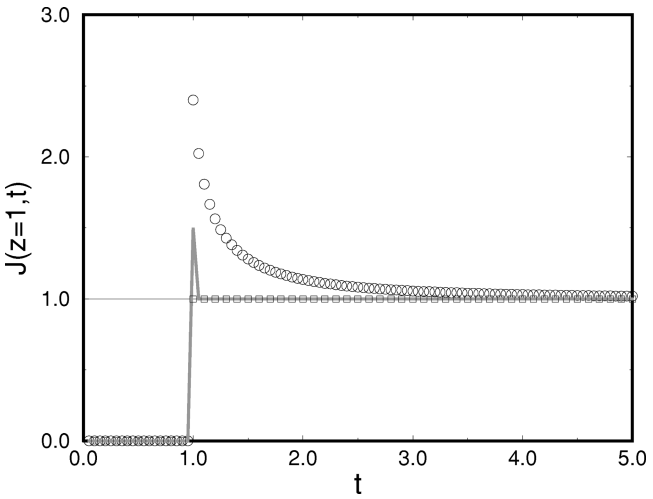

FIG. 3. Stress transfer kernels J for various models are shown as a function of time at a fixed distance $z=1$. The thin line is the kernel for the quasistatic model and the squares that for the sound-travel time-delayed monotonic model. The open circles represent the scalar elastic model with $\tau_0=0.01$, while the thick line represents the sharp pulse model with $\alpha=0.5$ and $\gamma=1.5$. For all except the quasistatic model, the stress transfer is zero for $t<z$.

This quasistatic model we study first. Its possible regimes of validity are discussed in Sec. V.

In order to separate the effects of sound-travel time delays from those of stress pulses, we also consider a model with monotonic stress transfer characterized by the kernel

$$J_{\text{td}}(z,t)=\frac{1}{\pi z^2}\Theta(t-|z|). \tag{37}$$

This kernel is similar to the quasistatic kernel except that the stress transfer is not instantaneous. Finally, in order to separate the effects of the maximum of the stress peaks from those of their tails, and to make the analysis of the stress peaks more tractable, we study a kernel with sharp pulses defined in Eq. (14). In both of these artificial models, the velocity of signal propagation has been set equal to one. Snapshots of the stress pulses when the crack front at $z=0$ is moved ahead by a small amount at $t=0$ and held there, are shown for the various models in Fig. 3. These are just plots of the respective $J(z,t)$ for a fixed t.

In general, the stress transfer along the crack front will depend on the shape of the front due to nonlinear terms in the expansion of $\mathcal{G}[\{f\}]$ in powers of f. Throughout this paper we will ignore these. We can justify this approximation for the quasistatic case for which we have an analytic understanding, and believe that it should generally be valid on long length and time scales as long as the crack front roughness exponent $\zeta<1$; i.e., that the crack front looks straight on asymptotically long scales.[13]

B. Numerical implementation

We are interested in the behavior of the crack front near to when it begins to move. Below and just above the critical load, the motion of the crack front is very jerky and segments of the crack front move ahead and then get stuck in a tougher region. The basic minimum length, time, and incre-

ment in the crack front position scales of these processes are set by the length scales of the toughness variations, the coefficient B in Eq. (26), etc. Thus to understand this behavior, it is natural to simulate the crack front in a manner which is discrete in space, time, and position.

Our simulations were done on a lattice which is periodic in the direction x of crack advance, but for each $z=0\cdots L-1$, the coordinate along the crack front, the row of points are shifted by an independent random amount, $b(z)$ with $0<b(z)<1$. The allowed values of the crack front position are thus

$$f(z)=b(z)+n(z) \tag{38}$$

with $n(z)$ integers. This avoids the possibility of lattice-locked behavior in which the crack advances in a relatively uniform manner characterized by all points advancing by one before any advance again, see discussion in Sec. VD. Periodic boundary conditions are used in the z direction. We have chosen the sound velocity in our models to be unity corresponding to one lattice spacing along the crack front per time step (all the models we study numerically have only one sound velocity).

At each lattice point an independent value of the random fracture toughness, $\gamma(x,z)$, is picked from the interval [0, 1.5]. This range is chosen so that the variations in γ are comparable to the force on points of the crack front on each other which are

$$g(z,t)=\sum_{z'=0}^{L-1}\sum_{t'\leq t}\tilde{J}(||z-z'||,t-t')\times[f(z',t')-f(z',t'-1)], \tag{39}$$

where, with the periodic boundary condition in z on a crack of length L;

$$||z-z'||\equiv\min(|z-z'|,|L-|z-z'||) \tag{40}$$

is the shortest distance between z and z'. The stress transfer kernels $\tilde{J}$ are modifications of the continuum kernels of interest with the stress pulses designed to die away smoothly after going through the system once. Thus, although there is a long-ranged history dependence in all but the quasistatic model, we need keep track of the history of the interface only up to a time corresponding to the sound-travel time through half the system, i.e., a time of $L/2$, where L is the system size. Thus,

$$\tilde{J}(z,t\geq L/2)=\tilde{J}(z,\infty)=\tilde{J}_{qs}(z)=\frac{1}{||z||^2} \tag{41}$$

for $z\neq 0$. The sum in Eq. (39) over $-\infty\leq t'\leq t-L/2-1$ can thus be replaced by $\Sigma_{z'}\tilde{J}(||z-z'||)f(z',t-L/2-1)$. Care must also be taken with the ''self-interaction'' piece $z=z'$ which represents the ''principal part'' in Eq. (30). In the quasistatic case (and generally for long time)

$$\tilde{J}(z=0,t)=-\sum_{z\neq 0}\tilde{J}_{qs}(||z||), \tag{42}$$

so that if the crack moves uniformly there are no changes in g. More generally, in particular for the artificial models, $\tilde{J}(z=0,t)$ involves some arbitrariness. To preserve the monotonicity of the sound-travel time-delayed model, a certain choice is required. This, and the detailed form of the various $\tilde{J}(z,t)$ used are specified in Appendix B. The evaluation of the elastic force at each time step is done in Fourier space using the fast Fourier time algorithm and hence the time for computation at each time step of the evolution of the interface scales like $L^2\ln L$.

The ''driving force'' $\mathcal{E}$ is the forcing parameter and as this is increased the crack begins to move. When the total ''force'' at a point z on the crack front is greater than the random part of the fracture toughness there, the crack front at z advances by one lattice constant, i.e.,

$$f(z,t+1)=f(z,t)+\Theta[g(z,t)-\gamma(z,t)+\mathcal{E}], \tag{43}$$

where the lattice constant is set equal to one and Θ is the step function.

These discrete automaton models for the crack front are expected to capture the physics at threshold of the corresponding continuum models at length scales long compared to the correlation length of the random toughness. Direct evidence for universality is provided by extensive numerical simulations on charge-density-wave models[17] in two dimensions which have found universal behavior for smooth and piecewise continuous pinning forces, as well as for discrete cellular automata analogous to the one defined above. We expect the same to hold here.

III. MONOTONIC MODELS

A. Quasistatic model

We first consider the quasistatic model. In this approximation, the stress transfer is instantaneous and the linearized continuum equation of motion of the crack front takes the form

$$\partial_t f(z,t)=\frac{1}{\pi}\mathcal{P}\int dz'\,\frac{f(z',t)-f(z,t)}{(z-z')^2}-\gamma[f(z,t),z]+\mathcal{E}. \tag{44}$$

Before presenting the numerical results from which we determine the values of various critical exponents characterizing the depinning transition, we give, following Refs. 3,4, scaling arguments for several identities between the exponents and bounds on them.

1. Exponent identities and bounds

In the moving phase, the crack front will be reasonably smooth at scales larger than the correlation length ξ, indeed at large scales $f\approx vt$ and hence the random toughness $\gamma(f,z)$ will act essentially like white noise and hence $\langle[f(z,t)-f(0,t)]^2\rangle\sim\ln(z)$. On scales smaller than ξ, the front will be rough with $|f(z,t)-f(0,t)|\sim|z|^{\zeta}$.

In order for the crack motion to be smooth on larger scales, each segment of the crack of length ξ must take about the same time $\tau\sim\xi^z$ the correlation time, to move through each distance ξ^{ζ}. In the region which a segment of length ξ passes through in time τ, there are $\xi^{\zeta+1}$ random values of the local toughness. This means that the force per unit length needed to pull the crack segment through this region must

vary from region to region by at least of order the random variation in the toughness averaged over this region, i.e., $1/\sqrt{\xi^{\zeta+1}}$ by the central limit theorem. Thus the course grained toughness variations at the scale ξ are

$$\delta\Gamma_\xi \gtrsim 1/\xi^{(\zeta+1)/2}. \tag{45}$$

The force on the segment from the external load and the rest of the crack must be just strong enough to overcome these random variations. If these forces were too strong, the segment would move more smoothly implying that it must have been longer than ξ by definition. On the other hand, if they were too weak, the segment would not move at all in some time intervals of length τ and thus it must have been smaller than ξ. Since the mean external load at which the segment moves is

$$G_c \equiv G_c^{qs}, \tag{46}$$

this implies that either

$$G^\infty - G_c \sim \delta\Gamma_\xi \gtrsim 1/\xi^{(\zeta+1)/2}, \tag{47}$$

i.e.,

$$\nu \geqslant \frac{2}{\zeta+1}, \tag{48}$$

or the force per unit length from the neighboring sections of the crack G_n are comparable to $\delta\Gamma_\xi$. The latter is dominated by nearby segments so that

$$G_n \sim \int_\xi^{2\xi} dz \frac{z^\zeta}{z^2} \sim \xi^{\zeta-1}, \tag{49}$$

yielding

$$\xi^{\zeta-1} \geqslant \frac{1}{\xi^{(\zeta+1)/2}} \tag{50}$$

and hence,

$$\zeta \geqslant 1/3. \tag{51}$$

If there is only one basic scale of the forces near threshold, as simple scaling would suggest, then we should expect that

$$G^\infty - G_c \sim G_n \sim \delta\Gamma_\xi. \tag{52}$$

The rough equality of the typical force per unit length G_m of a segment of length ξ on a segment a distance ξ away and $G^\infty - G_c$ thereby yields the scaling relation

$$\nu = \frac{1}{1-\zeta}. \tag{53}$$

Similar argument can be used below threshold implying that the correlation length exponents on the two sides of the transition are equal.[3] We will derive the relation Eq. (53) more directly below.

The bound on ν, Eq. (48), comes from an argument similar to that by Harris[18] for equilibrium phase transitions and established more generally in Ref. 19. We can also derive it by considering some segment of the crack front of size ξ_- below the threshold, loosely defining $G_\xi^c = G_c + \delta\Gamma_\xi$ to be the local critical force at which this segment begins to move. Below threshold, segments of size of order ξ have a substantial chance both of having already moved or not having moved yet while G^∞ was increased to its present value. Thus the variations in G_ξ^c must be comparable to $G_c - G^\infty$. This is similar to what was argued for above G_c, but here it does not rely on as many assumptions about scaling. Since $\delta\Gamma_\xi \gtrsim 1/\xi_-^{(1+\zeta)/2}$, we obtain Eq. (48) just as from above threshold.

We now obtain scaling relations for the distribution of avalanche sizes below the threshold loading. Following Ref. 3 we conjecture that the distribution of avalanches as G^∞ is increased slightly has a scaling form

$$\text{Fraction of avalanches with size} > l$$
$$\text{when } G^\infty \to G^\infty + dG^\infty \approx \frac{1}{l^\kappa}\hat{\rho}(l/\xi_-) \tag{54}$$

at a given external load, with $\xi_- \sim (G_c - G^\infty)^{-\nu}$. Following the same reference we obtain

$$\kappa = 1 - 1/\nu \tag{55}$$

from the increase in the mean position as G_c is approached. Now consider the probability distribution of the size of *all* avalanches that occur on sweeping the load from zero to the threshold load,

$$\text{Fraction of all avalanches with size } > l$$
$$\approx \int_0^{G_c} \frac{1}{l^\kappa}\hat{\rho}(l/\xi_-) n_A(G^\infty) dG^\infty \sim l^{-\kappa-1/\nu} = l^{-1}, \tag{56}$$

where the last equality was obtained using the scaling relation Eq. (55) and the observation that the rate of avalanche production, $n_A(G^\infty)$, per increase in G^∞ goes to a const at G_c. Thus,

$$\text{Prob(size of a given avalanche} = l) \sim 1/l^2. \tag{57}$$

An exponent identity relating the velocity exponent β to the other exponents follows directly from the picture discussed above of the moving segments of length ξ. Since the time for a segment of length ξ to move ahead a distance which scales as ξ^ζ, is of order ξ^z, the velocity of the interface scales as $\xi^{\zeta-z}$. We thus obtain

$$\beta = (z-\zeta)\nu. \tag{58}$$

Another useful relation can be obtained by considering adding an additional ''force,'' $\epsilon(z,t)$, on the crack front. Denoting the resulting change $\delta f(z,t)$, we can define the polarizability χ as

$$\chi(k,\omega) = \frac{\delta\langle f(k,\omega)\rangle}{\delta\epsilon(k,\omega)} \tag{59}$$

in Fourier space. First consider applying a static force. In this case the additional force $\epsilon(k,\omega)$ can be absorbed by redefining

$$f(k,\omega) \to f'(k,\omega) - \frac{\epsilon(k)}{|k|}, \tag{60}$$

since the terms from the interaction of the crack front with itself in the equation of motion will then exactly cancel the additional force ϵ. The statistics of the random toughness variables, in this distorted frame,

$$\gamma'(x,z)=\gamma[x+\phi(z),z], \tag{61}$$

with $\phi(z)$ the Fourier transform of $\epsilon(k)/|k|$, will have the *same statistics* as the original ones. This is an important *statistical symmetry* of the system. It is the small-angle form of the statistical rotational invariance. We thus have $\delta\langle f(k,\omega)\rangle=\epsilon(k)/|k|$, and hence

$$\chi(k,0)=\frac{1}{|k|} \tag{62}$$

exactly. On the other hand, on applying a low-frequency spatially uniform force $\epsilon(\omega)$, we should have

$$-i\omega\chi(0,\omega)=\frac{dv}{d\epsilon}\sim(G^{\infty}-G_c)^{\beta-1}. \tag{63}$$

Generally, we expect that $\chi(k,\omega)$ will have the scaling form

$$\chi(k,\omega)\sim\frac{(G^{\infty}-G_c)^{\beta-1}}{-i\omega}X(k\xi,\omega\xi^z) \tag{64}$$

with the form of the prefactors implied by Eq. (63). In the static limit, $X(k\xi,u=0)=0$, and

$$\lim_{\omega\to 0}\chi(k,\omega)\sim\xi^z(G^{\infty}-G_c)^{\beta-1}i\left.\frac{\partial X(k\xi,u)}{\partial u}\right|_{u=0}. \tag{65}$$

Comparing Eqs. (62) and (65) we see that

$$\frac{\xi^z(G^{\infty}-G_c)^{\beta-1}}{|k|\xi}\sim\frac{1}{|k|}. \tag{66}$$

But since $\xi\sim(G^{\infty}-G_c)^{-\nu}$, we have

$$\beta-1-\nu(z-1)=0. \tag{67}$$

Using the expression for β from Eq. (58) we again obtain Eq. (53). As noted above, this simply relates the force of length ξ segments on each other to $G^{\infty}-G_c$.

We thus have two independent exponents from which the others can be obtained. In addition, from Eqs. (48) and (58) we obtain the bounds

$$\zeta\geqslant 1/3, \tag{68}$$

and hence

$$\nu\geqslant 3/2. \tag{69}$$

All of the exponent identities and the form of scaling functions such as Eq. (64) have been derived from a renormalization-group expansion about two dimensions which is the critical dimension for the depinning transition of manifolds driven through random media with long-range interactions decaying as $1/r^{d+1}$,—i.e., $|k|$ in Fourier space.[20] The analytical results from the $d=2-\varepsilon$ expansion are compared with our numerical results in the next subsection.

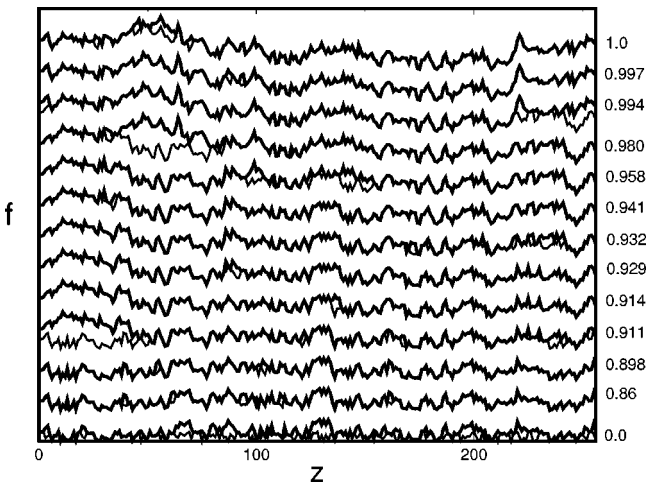

FIG. 4. Series of avalanches in the quasistatic model in a system of size 256, as the load is gradually increased by just enough at each step to trigger the most weakly pinned site. The system is then allowed to evolve until motion stops before the load is increased again. The configuration of the crack front is shown by a thin line at the begining and by a thick line at the end of each avalanche to demarcate the sites which have moved. The position of the crack front in the figure is displaced vertically by a constant factor after each avalanche to differentiate between the individual avalanches. The initial almost straight configuration of the crack front at zero load is also shown. The avalanches shown occur at fractional loads (indicated on the right) in the range from 0.86 of the threshold load to the threshold load at which point the crack front starts moving.

2. Numerical results

We now present the numerical results for the quasistatic model from which we obtain the values of the various exponents. As discussed earlier, we simulate a discretized version of this equation, here simply

$$f(z,t+1)=f(z,t)+\Theta\left[\sum_{z=0}^{L-1}\frac{f(z',t)-f(z,t)}{||z-z'||^2}-\gamma(z,t)+\mathcal{E}\right], \tag{70}$$

where L is the system size, to study the dynamics at threshold. We start with a pinned configuration of the crack front that is as close as possible to being straight and gradually increase the load until the most weakly pinned point becomes unstable and jumps. This point, in turn, may pull along other points on the crack front due to the elastic interactions, causing an avalanche. During the avalanche, the load is held fixed. Once the avalanche subsides, the load is increased once again until another point becomes unstable, and so on. A series of avalanches, as the load is gradually increased in this way is shown in Fig. 4. A space-time plot of one of the large avalanches is shown in Fig. 5.

Defining the *size* of an avalanche is somewhat problematic. We have chosen to define it as the number of distinct points on the crack front that move during the course of the avalanche. Note that various other ways of defining the ''size'' of an avalanche along the crack front by, e.g., its ''moment of inertia'' about its center of mass or by its maximum extent have problems because of the power-law tail of the interactions which can trigger some jumps far away. In addition, periodic boundary conditions would complicate a

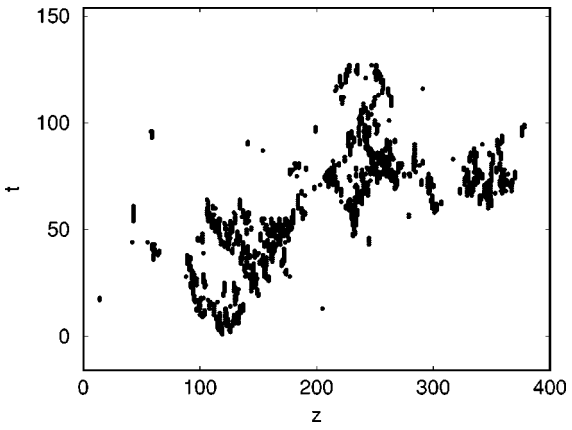

FIG. 5. Space-time plot of a large avalanche in the quasistatic model in a system of size 512, with the points on the interface which moved ahead at each instant of time indicated.

definition. To study the statistics of many avalanches, the avalanche sizes are binned in powers of 2. To measure the dynamic exponent z, statistics of avalanche sizes versus their durations are collected for all the avalanches that occur as the load is increased from zero to the critical load. The log-log plot of the number of avalanches in a given bin against the bin size is shown in Fig. 6 and a linear fit gives us a slope of 2.14 ± 0.3 in agreement with Eq. (57) but with large errors.

Figure 7 shows the plot of the mean duration of avalanches in a bin $\tau_{\rm bin}$ versus bin size $l_{\rm bin}$, for a system of length 1024. From the slope of the log-log plot we determine

$$z=0.74\pm0.03. \tag{71}$$

As is generally true, one must be very careful not to take such statistical estimates of uncertainties in exponents at face value due to the existence of corrections to scaling. Fortunately, in our case, the $2-\varepsilon$ expansion provides an estimate of the leading correction to scaling exponent; the calculations of Narayan[21] yield the leading irrelevant eigenvalue at the critical fixed point to be approximately $-\varepsilon/3\approx-1/3$ in our case with $\varepsilon=1$. We thus fit the data to the form $\tau_{\rm bin}=Cl_{\rm bin}^{z}/(1+A_z l_{\rm bin}^{-1/3})$ and find that $A_z\ll1$ and hence this fit gives the same value of z to within error bars.

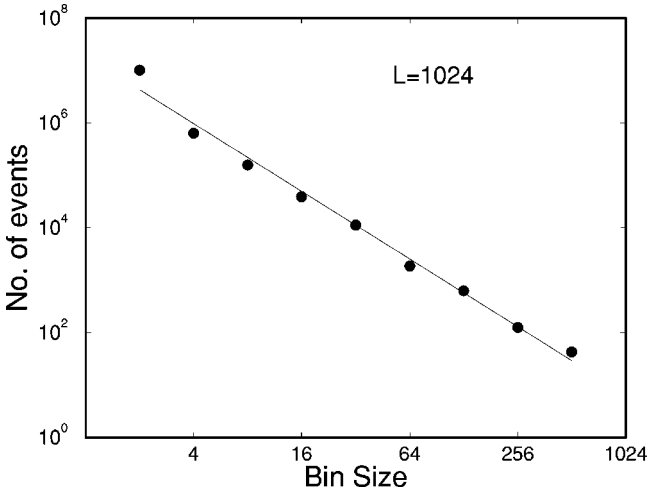

FIG. 6. As the load is increased from zero towards the critical load, the avalanches that occur in the quasistatic model are binned according to their size, which is defined as the number of distinct sites that move during an avalanche. The bin is defined by (bin size)/$\sqrt{2}<$avalanche size$\leqslant\sqrt{2}$(bin size). The number of avalanches in each bin are plotted versus the bin size for systems of size 1024. The slope of the log-log plot is 2.14 ± 0.3.

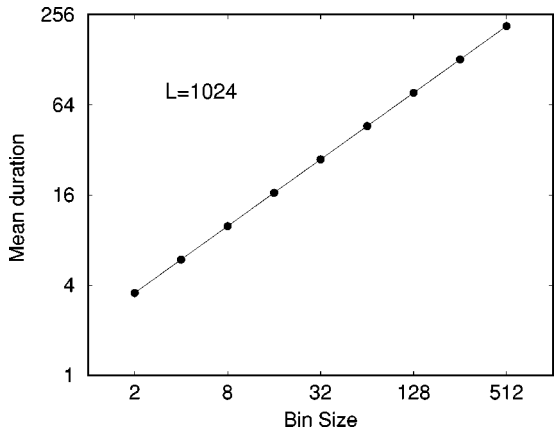

FIG. 7. Log-log plot of the mean duration of an avalanche versus the bin size is shown for the quasistatic model with system size 1024. The avalanches are binned according to their size which is determined by the number of sites that moved during that avalanche. The nth bin is defined by (bin size)/$\sqrt{2}<$avalanche size $\leqslant\sqrt{2}$(bin size). The slope of the graph yields a dynamic critical exponent of $z=0.74\pm0.03$.

From the ε expansion,[3,4] it was found that

$$z\approx1-2\varepsilon/9+\mathcal{O}(\varepsilon^2)\approx7/9\approx0.78 \tag{72}$$

for $\varepsilon=2-d=1$. If we neglect the $\mathcal{O}(\varepsilon^2)$ and higher terms, this agrees with our numerical result within error bars.

In a finite system, there is some ambiguity in the definition of the critical load. For example, if the system extends very far in the direction of motion, the whole crack front would typically move from its initial position but get stuck in a rare tough region far away. In order not to bias the results by choice of the system extent in the direction of motion, we define the critical load as the load at which every point but one on the interface has moved at least once. For a large system we find

$$G_c\approx0.97. \tag{73}$$

Note that the random forces, the critical driving force and the nearest-neighbor elastic forces are very comparable.

Right at threshold the crack front is found to be self-affine as expected. Figure 8 shows the plot of the power spectrum of the crack front $\langle|f(k)|^2\rangle$ at threshold, as a function of the wave vector for various system sizes ranging from 4 to 4096. We expect the power spectrum to be $k^{-(2\zeta+1)}$ for small k. The best fit to a straight line is shown in Fig. 9 for a system size of 4096 averaged over 1000 samples. The slope of this line gives us $2\zeta+1$, from which we determine

$$\zeta=0.34\pm0.02. \tag{74}$$

Surprisingly, even at very small wave vectors, the power spectrum still looks linear on a log-log plot and we do not see significant finite-size effects even at the wave vector corresponding to half the system size. Since the data in Fig. 9 have very small statistical uncertainties, we can try to fit the

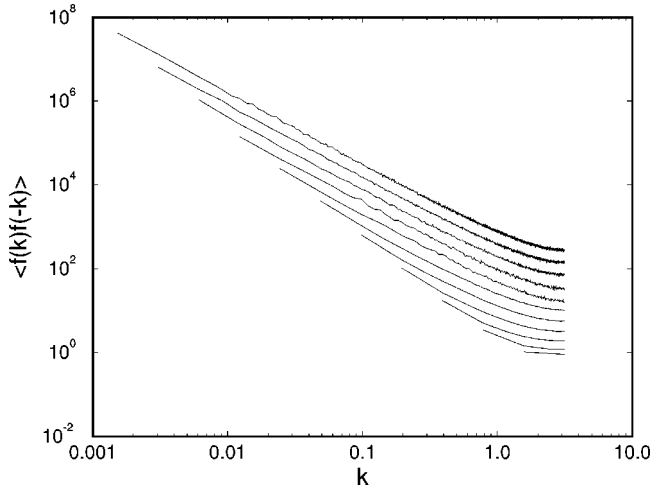

FIG. 8. Log-log plot of the power spectrum versus the wave vector is shown for systems at the quasistatic critical load, ranging in size from 4 to 4096. They have been shifted along the vertical axis for clarity.

power spectrum to the form $Ck^{-(2\zeta+1)}(1+A_\zeta k^{1/3})$ using corrections to scaling. The coefficient A_ζ turns out to be very small and we obtain the same roughness exponent with comparable error bars. This gives us some confidence in the estimate Eq. (74).

Our result for ζ satisfies, and may saturate, the bound $\zeta \geqslant 1/3$. The prediction of ζ from the ε expansion is

$$\zeta = \varepsilon/3 + o(\varepsilon^n) \tag{75}$$

for all n,[3] i.e., there appears to be no corrections to all orders in ε although ''nonperturbative'' corrections cannot be ruled out. Nevertheless, the bound Eq. (68), the ε expansion result Eq. (75), and the numerics suggest that perhaps ζ may be exactly 1/3 although at this point we know of no solid argument that yields 1/3 as an upper (to complement the lower) bound.

The correlation exponent ν can be obtained via the finite-size scaling hypothesis by measuring the variance of the threshold load $G_c(L)$ as a function of the system size. Assuming that there is only one important length scale ξ, the variance of the threshold force $[\Delta G_c(L)]^2$ scales with the system length L as

$$[\Delta G_c(L)]^2 \sim L^{-2/\nu}. \tag{76}$$

A direct fit to $L^{-1/\nu}$ of the plot in Fig. 10 of the variance of the threshold load versus the system size, for system lengths ranging from 4 to 8192, leads to $\nu = 1.80 \pm 0.05$, while a fit for system lengths ranging from 256 to 8192, gives $\nu = 1.72 \pm 0.12$. But a systematic curvature can be seen. In light of the knowledge of the corrections to scaling, we can do better by fitting to the form $CL^{-1/\nu}/(1+A_\nu L^{-1/3})$ from which obtain

$$\nu = 1.52 \pm 0.02. \tag{77}$$

This fit is shown in Fig. 11 for systems of length 4 to 8192 lattice constants. In this case, as suggested by the data, A_ν is not small and the fit indeed yields $A_\nu = 0.87$. Note that the expected scaling equality Eq. (53) is obeyed, but *only when the corrections to scaling are included.*

As the load is increased above threshold, the crack front begins to move. As for the critical load, we must be careful

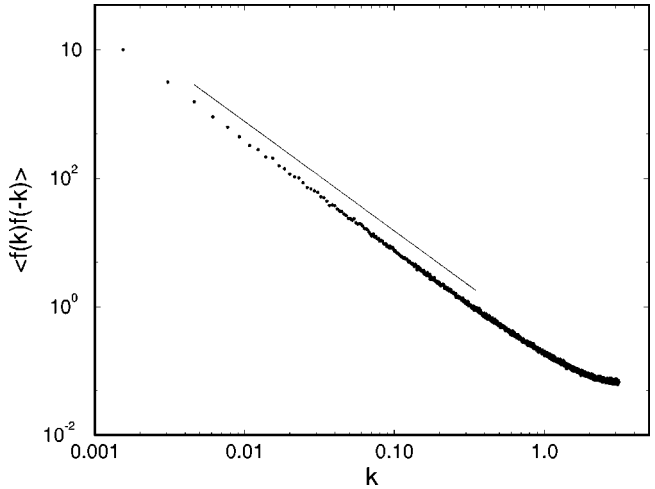

FIG. 9. Log-log plot of the power spectrum for system size 4096, averaged over 1000 samples and a linear fit over $0.004 \leqslant k \leqslant 0.35$ which leads to $2\zeta + 1 = 1.68 \pm 0.04$.

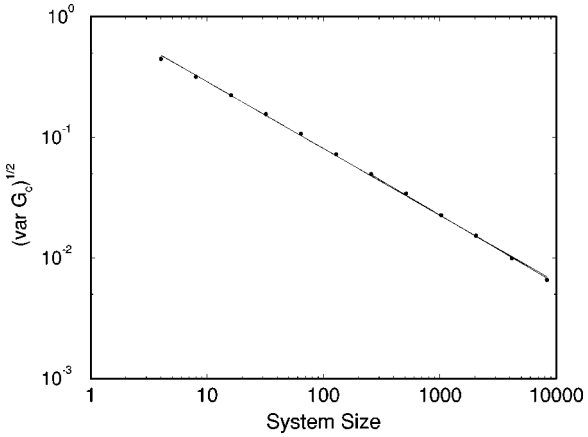

FIG. 10. Log-log plot of the variance of the quasistatic threshold load as a function of the system size in the range from 4 to 8096. From a linear fit over the full range, $\nu = 1.80 \pm 0.05$, while a fit for sizes from 256 to 8096 yields $\nu = 1.72 \pm 0.12$.

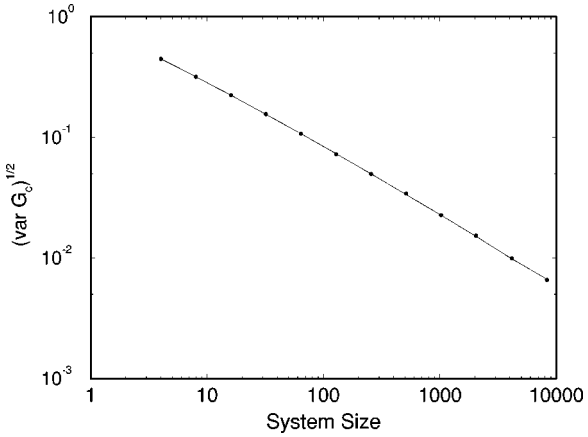

FIG. 11. Best fit of the variance of the quasistatic threshold load as a function of the system size to the form $CL^{-1/\nu}/(1+A_\nu L^{-1/3})$. This yields $\nu = 1.52 \pm 0.02$ and $A_\nu = 0.87 \pm 0.03$.

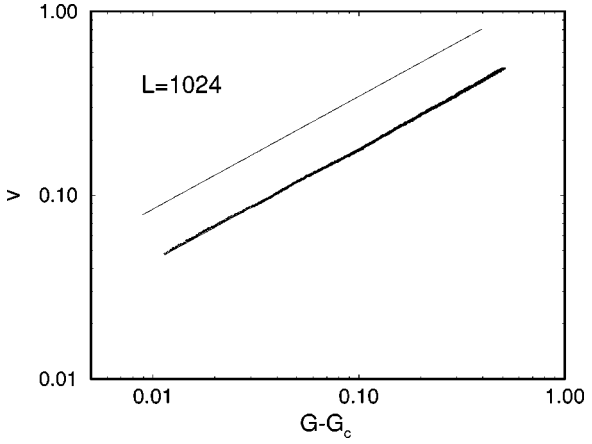

FIG. 12. Log-log plot of the mean velocity in the quasistatic model versus the the excess of the load above the critical value. The slope yields $\beta = 0.68 \pm 0.06$.

how we define the velocity for finite length crack fronts. If we choose a system of great extent, W, in the direction of motion, the front will tend to get stuck in anomalously tough regions; this effect will be more pronounced for small L. But since we are interested in the critical behavior and we have a good handle on the scaling of f with L, we can instead choose systems of extent $W \approx C_W L^{\zeta}$ with periodic boundary conditions in the direction of motion. For monotonic models, the convexity then implies convergence to a unique steady state.[10] Since at threshold $\Delta f \sim L^{\zeta}$ with a coefficient roughly of order unity, we choose $C_W = 4$.

There is a complication that must be considered: due to the possibility of a pinned configuration for loads above that at which the last point became depinned, the minimum G^{∞} at which $v > 0$ will sometimes be greater than our definition of G_c by a random amount whose distribution depends on C_W. From scaling we expect

$$G_{\min}^{\text{moving}} - G_c \sim 1/L^{1/\nu}. \tag{78}$$

By scaling, there will thus be a typical minimum velocity

$$v_{\min} \sim 1/L^{\beta/\nu} \sim 1/L^{z-\zeta}. \tag{79}$$

Note that the minimum velocity due to the discreteness of time is much less than this and hence negligible for large L.

Figure 12 shows a plot of the mean velocity of the front as a function of the loading for a system of length 1024 from which we determine

$$\beta = 0.68 \pm 0.06. \tag{80}$$

The fit using the corrections to scaling leads to the same value of β within the error bars. Surprisingly, there do not seem to be substantial deviations for $G \geqslant G_{\min}^{\text{moving}}$.

The ε-expansion prediction is $\beta \simeq 2/3$ if we use $\zeta = 1/3$ and $z = 7/9$; again there is reasonably good agreement between our numerical results and the ε expansion although our error bars are larger for β than for z, ν or ζ.

In our numerical results, the critical force and all of the coefficients in scaling laws are of order unity suggesting that we have no intermediate length, displacement or time scales and thus that the scaling should work well for all but small size samples. If we had chosen too narrow a distribution of random toughness $\gamma(x,z)$, there would have been an intermediate length scale and this would no longer have been the case. Note that the renormalization-group methods can be used to show that nonlinearities associated with higher-order terms in the expansion of $\mathcal{G}[\{f\}]$ are, for quasistatic stress transfer, irrelevant for the critical behavior. One could have guessed this since, from the homogeneity of $\mathcal{G}[\{f\}]$ higher powers of f have an equivalent number of powers of gradients, so that $\zeta < 1$ implies that they are irrelevant.

B. Monotonic model with time-delayed interaction

In the previous section, we saw that the quasistatic approximation to stress transfer gave rise to a critical depinning transition with a dynamic exponent $z < 1$. This means that for large enough avalanches which typically occur only if the load is close enough to G_c, the effective disturbance velocity of an avalanche of size l will be l/l^z times the basic microscopic velocity scale of disturbances set by the dissipative coefficient B in Eq. (29). Thus for sufficiently large l, the quasistatic avalanches will progress faster than the sound speed. This is clearly unphysical and in this regime, the sound travel-time delays in the stress transfer must play a role. In order to understand the effects of these and of stress overshoots separately, we study a monotonic model—i.e., with no stress overshoots—but with sound-travel time delays. The simplest form of this is to simply replace the $\Theta(z)$ in the quasistatic stress transfer with $\Theta(t-|z|)$. On a lattice the stress transfer kernel becomes

$$J_{\text{td}}(z,t) = \frac{\Theta(t-||z||)}{||z||^2}(1-\delta_{z,0}) - \delta_{z,0} \sum_{z' \neq 0} \frac{1}{||z||'^2}. \tag{81}$$

Some care is needed in choosing the second, local, term in Eq. (81). The natural choice would be to fix $J(z=0,t)$ by the condition that for all times, $\Sigma_z J(z,t) = 0$. This condition is satisfied for the quasistatic model and for the scalar model as well as for real elasticity. It ensures that for a straight crack, the instantaneous crack front velocity is a function solely of the instantaneous external load and independent of the past history of the crack, since for a straight crack the effect of the crack front interactions vanishes at all times. If we made $\Sigma_z J(z,t) = 0$ here also, however, Eq. (81) would no longer be monotonic. Rather, the stress at a point z, after a jump at the same point, would decrease in time as the integrated stress transferred to the rest of the crack increases; this would act like a stress overshoot. For now we will, therefore, give up the independence of a straight crack on its past history to preserve the monotonicity condition.

We see that in this model the force on any given point on the crack front at any given time is always less than or equal to the equivalent force for the same configuration in the quasistatic model. Note also that for a crack front which is stationary after some time t, in the discrete-time periodic boundary-condition version of this model (see Appendix B), the force at all points on the crack front, will reach the quasistatic value by time $t + L/2$. As shown in Appendix A, these conditions imply that if the external load is increased adiabatically from the same initial conditions, the time-delayed model, Eq. (81), has *exactly the same static properties* as the quasistatic model. Indeed, for a given realization

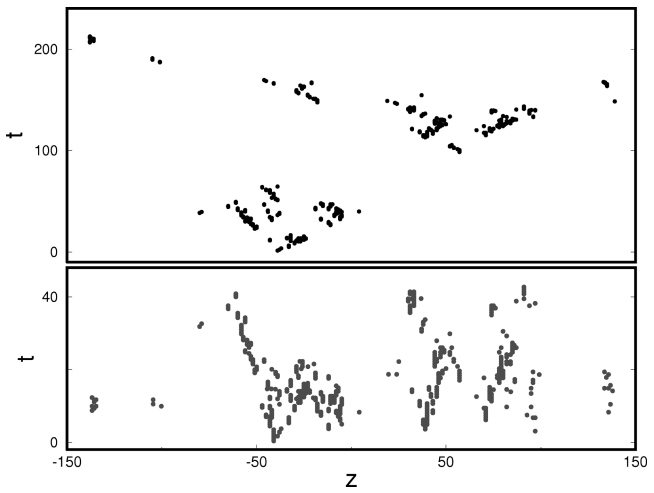

FIG. 13. Space-time plot of an avalanche for (a) the time-delayed monotonic model (top) and (b) for the quasistatic model (bottom) starting from the same initial configuration of the crack front. The sets of jumps in the two figures are identical, but they occur at different times.

of the random toughness, every finite avalanche that occurs in the two models will be identical, except for the times at which points on the crack front jump. Therefore, both the models will have identical threshold forces, and the exponents ν and ζ are then obviously identical to their quasistatic values.

The space-time plot of a particular avalanche as one site is triggered by increasing the load, is shown in Fig. 13 for the quasistatic model and of the identical avalanche in the sound-travel time-delayed model starting from the same initial configuration of the crack front in a system of length 512. It is evident that the dynamics of the avalanches in the two models is very different.

The Fourier transform of the continuum version of the time-delayed kernel in Eq. (81) is given by

$$J(k,\omega)=-\frac{1}{i\omega}\Bigg\{-\frac{i}{\pi}(k+\omega)\ln|k+\omega|+\frac{i}{\pi}(k-\omega)\ln|k-\omega| -\frac{1}{2}|k+\omega|-\frac{1}{2}|k-\omega|\Bigg\}+U(\omega), \tag{82}$$

where there is an ambiguity in the uniform $k=0$ part of the Fourier transform $U(\omega)$. It is clear that the dynamic exponent must be $z\geqslant 1$. Let us assume that $z>1$ or more precisely that the characteristic time $\tau\gg\xi$ near threshold. We are thus interested in the behavior in the scaling limit in which $|\omega|\ll|k|$. In this limit

$$J(k,\omega)\approx\frac{2}{\pi}\ln|k|+\frac{|k|}{i\omega}. \tag{83}$$

From the equation of motion, the response function defined in Eq. (59) is in the absence of the randomness

$$\chi=\frac{1}{-i\omega B+i\omega J(k,\omega)}\approx\frac{1}{-i\omega(2/\pi)\ln(1/|k|)+|k|} \tag{84}$$

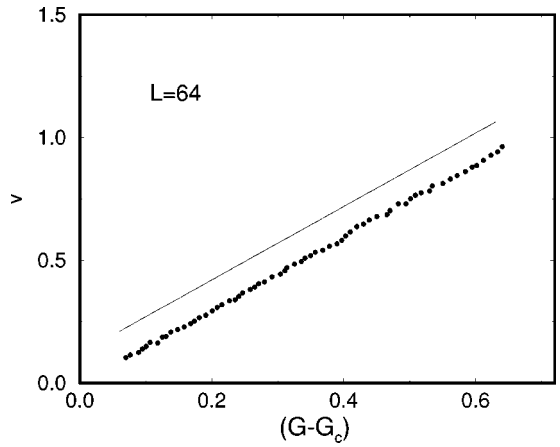

FIG. 14. Velocity versus load for the time-delayed monotonic kernel in a system of size 64, and a linear fit to the data.

for $\omega\ll k$, since the $\ln|k|$ term from J will dominate the ω dependence. In mean-field theory, this gives rise to times scaling with lengths as

$$\tau\sim\xi\ln\xi. \tag{85}$$

In the absence of the $\ln|k|$, renormalization due to the random roughness would make $B_{\rm eff}$ decrease with length scale in $2-\varepsilon$ dimensions. However, the $\ln|k|$, being singular, cannot renormalize. But it *can* feed into the renormalization of B. Following this through yields

$$\tau_\xi\sim\tilde{c}\xi \tag{86}$$

in dimensions $d=2-\varepsilon$ with $\tilde{c}$ an effective velocity of order ε for small ε, but presumably of order unity in our one-dimensional case. Thus we see that assuming $z>1$ leads back to

$$z=1, \tag{87}$$

which we believe should be correct with *no* logarithmic corrections. Using the exponent identities Eqs. (58) and (53) we obtain

$$\beta=1. \tag{88}$$

A plot of the load versus the mean crack velocity is shown in Fig. 14 for a system of size 64. It is very close to linear although the range is small enough that one cannot reliably extract β. Note that because of the dependence on the past history, we are limited here to rather small samples. While the computations for each time step for the quasistatic model take a time of order $L\ln L$, those for the sound-travel time-delayed model take $L^2\ln L$ and hence even for a system of length 64, the statistics are more difficult to obtain.

IV. STRESS OVERSHOOTS: NONMONOTONIC KERNELS

We now turn to more realistic stress transfer kernels. We have seen from Eqs. (34) and (23), that bulk sound modes naturally lead to nonmonotonic kernels of the stress transfer along the crack front. A regime of negative stress transfer, as occurs at intermediate times for tensile cracks, cannot by itself, change the behavior much from the time-delayed monotonic models since, in the absence of stress overshoots,

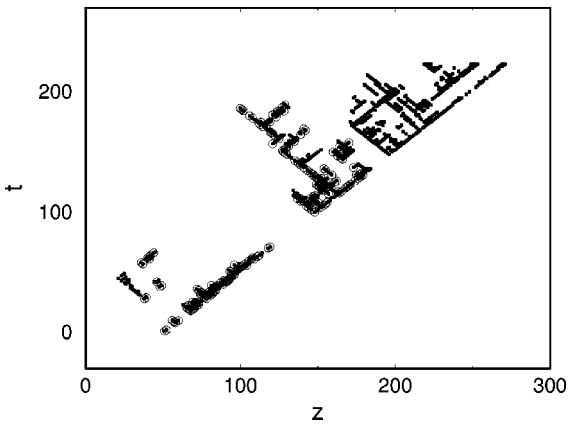

FIG. 15. Space-time plot of an avalanche for the time-delayed monotonic model (open circles) and the stress pulse model with $\alpha=0.5, \gamma=1.5$ (with dots) from identical initial conditions. It can be seen that a large number of additional sites jump for the model with stress overshoots.

the static behavior will again be identical to the quasistatic model. Thus the primary differences between the time-delayed model and more realistic models must be associated with the stress overshoots. The actual shape of the stress overshoot may be complicated by various factors including the effects of multiple scattering of sound waves off the crack front. Therefore, we would like to understand what features of the stress overshoot play a crucial role in the dynamics near threshold. To do this, we study simpler models and hope that the conclusions drawn from these models will help us understand the case of real elastodynamics.

A. Sharp stress pulses

We first consider a simple model of the overshoots in which sharp stress pulse travels with the sound speed. We take the amplitude of the overshoot to decay as a power law of distance as it moves along the crack front. The continuum version of the kernel we study has the form

$$J_{\rm sp}(z,t;\alpha,\gamma)=\Theta(t-|z|)/z^2+\alpha\,\delta(t-|z|)/|z|^{\gamma}. \quad (89)$$

This kernel reduces to the previous case of the monotonic time-delayed interactions when $\alpha=0$.

In Fig. 15 a large avalanche that occurs on triggering the most weakly pinned site is shown for both the monotonic time-delayed kernel and for the kernel $J_{\rm sp}(z,t;\alpha=0.5,\ \gamma=1.5)$ starting from the same initial configuration of the crack front and the same configuration of random toughnesses. We see that in the presence of the overshoot many more sites are triggered than for the monotonic kernel. Our data show that even for small overshoots their effects build and cause sufficiently large avalanches to run away. This causes the crack front to depin and start moving at a threshold load which is less than the one for the quasistatic stress transfer.

We find that for any value of γ and any nonzero α, the threshold load $G_c(\alpha,\gamma)$ is lower than $G_c(\alpha=0,\gamma)=G_c^{qs}$. A plot of $\langle G_c^{qs}-G_c(\alpha,\gamma)\rangle$ as a function of α^2 is shown in Fig. 16 for various values of γ, including $\gamma=\infty$, for which only the nearest neighbor of a jumped site feels the overshoot. The shift in threshold load from G_c was obtained by averaging over the *same* set of random samples with and without the overshoot; this greatly reduces the error bars. The value of G_c can be accurately determined from the quasistatic model where the code is much less numerically intensive. For all the values of γ studied, $\gamma\geqslant 0.5$, we find results consistent with

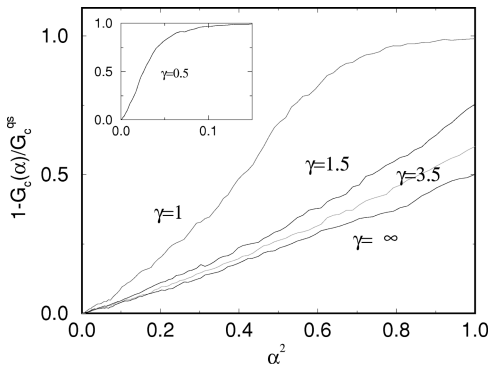

FIG. 16. The fractional decrease in the threshold load, $1-G_c(\alpha,\gamma)/G_c^{qs}$ for a system of size 64, is plotted as a function of α^2 for $\gamma=0.5$, 1, 1.5, 3.5, and ∞.

$$G_c^{qs}-G_c(\alpha,\gamma)\sim\alpha^2 \quad (90)$$

for small α, a form which will be derived below. Thus the overshoot appears to always be *relevant* at the quastatic depinning fixed point.

One of the advantages of starting with monotonic models for which we have quite a detailed understanding, is that the effects of perturbations away from these can be analyzed using known scaling properties of the monotonic models. We would like to carry this out for weak stress pulses added to the time-delayed monotonic model; i.e., to consider the behavior of the crack with stress transfer given by Eq. (89) for small α. In order to do this we first obtain the response to a *single* stress overshoot.

We focus on a given space-time point, at (Z,T) which we denote ''A'' and an avalanche that started at (0,0) in the time-delayed model without stress pulses. For simplicity we restrict consideration initially to $\gamma\to\infty$ so that only the nearest neighbor of a jump site will feel a stress pulse which will be α above the static stress. In order for A to be affected, one of the two neighboring sites of A, say $Z-1$, must have jumped at time $T-1$ producing a pulse; denote this space-time point ''P.'' Three conditions must be met for A to be affected by the stress pulse from $Z-1$, i.e., for point Z to jump an extra time. First, A must be within α of jumping anyway for the stress pulse to have been able to trigger its jump. The force increment needed for individual sites to jump are uniformly distributed for sites near to jumping, so the probability of this is simply of order α. Second, the increase in stress at site Z *after* time T must be less than α, or else the site would have jumped again regardless; denote this condition ''L''(for ''later stress''). Third, the neighbor must jump at $T-1$, i.e., the jump P must occur.

The scaling properties of avalanches imply that within the space-time volume of a large avalanche, there are holes on all scales (since $l^{\zeta}l\ll l^2$) and subavalanches of all sizes; see Fig. 13(a). Consider a subavalanche that occurs in a region within a time $\tau\ll T$ before P and within distance of order τ

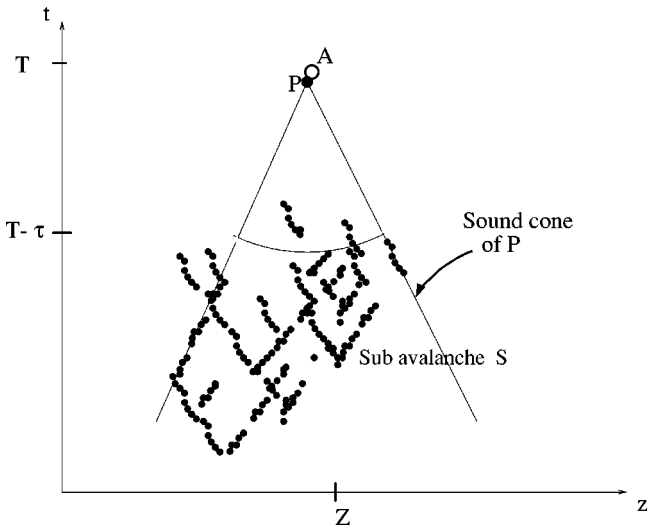

FIG. 17. Schematic of situation used in estimating the effects of a single small stress pulse. The space-time point A at which we estimate the probability of an additional jump due to a stress pulse from its neighbor jumping at a space-time point P, and P's ''sound cone'' showing P's isolation from the subavalanche S by a scale τ are all shown.

from P that is mostly contained within the ''backward sound cone'' of P, as shown in Fig. 17. If P is not well enough ''isolated'' from the bulk of this subavalanche, then we must consider a smaller subavalanche until we find the largest τ such that there is a subavalanche with size of order τ from which P is ''isolated'' in space time by order τ (if this does not exist, then it is highly unlikely that condition L can be satisfied). By isolated, we mean that there are few (or no) jumps on or outside of the backwards sound cone of P—''P's cone''—within a time τ. This is illustrated in Fig. 17. The maximal such subavalanche which we denote ''S'' typically has of order $\tau^{1+\zeta}$ jumps of which a fraction $1/\tau$, i.e., τ^{ζ}, are on P's sound cone. Since these are typically a distance $\gtrsim\tau$ from Z, they each cause the stress at P to increase by order $1/\tau^2$. Thus the isolated space-time point P will typically have a stress increase of $1/\tau^{2-\zeta}$ (between time $T-2$ and $T-1$) due to the subavalanche S, the probability of a jump at P given S is of this same order.

The condition that P is isolated from S is not a stringent one. Any jump in S outside of $A's$ cone (which is almost identical to P's cone) will cause a stress increase Δ_L at Z after time T. Since there will be of order $\tau^{1+\zeta}$ such jumps, each yielding a stress increase at Z of order $1/\tau^2$, Δ_L will be of order $1/\tau^{1-\zeta}$. This stress increase will be larger than α, and hence violate condition L, unless $\tau>1/\alpha^{1/(1-\zeta)}$ (note that obtaining this condition by either a smaller subavalanche with anomalously few jumps outside of A's cone or by P being less isolated from S is very unlikely). The probability of both satisfying the condition L that the stress increase after T be small *and* having a jump at P, is thus controlled by the smallest τ

$$\tau_\alpha\sim 1/\alpha^{1/(1-\zeta)} \tag{91}$$

for which L is satisfied with reasonable probability. The relevant subavalanches S are thus of size of order τ_α and occur in a space-time region of extent $\tau_\alpha\times\tau_\alpha$ near P. Since L is then quite probable

$$\text{Prob}[\text{jump at } P \text{ and } L|\text{size } (S)\sim\tau_\alpha] \sim 1/\tau_\alpha^{2-\zeta}\sim\alpha^{1+1/(1-\zeta)}, \tag{92}$$

which is simply proportional to the increase in stress at P due to S.

What is the chance that there is such an appropriate subavalanche S in the space-time region within τ_α of P? If there is any activity in this region, then it should include subavalanches on all scales, but we also need this to be the *last* activity in this region (or else L will be violated). If T is of order the duration of the full avalanche, the last activity in this region could occur anywhere within a time of order T. Thus

$$\text{Prob}(\text{last activity being within } \tau_\alpha \text{ of } T)\sim\tau_\alpha/T. \tag{93}$$

We obtain the probability of a pulse-triggered extra jump at A by combining all the factors from Eqs. (92),(93), and the probability α of site Z being close to jumping again, yielding

$$\text{Prob}(\text{pulse triggering extra jump at } A| \text{ avalanche of size}\sim T)\sim\frac{1}{\tau_\alpha^{2-\zeta}}\frac{\tau_\alpha}{T}\alpha\sim\frac{\alpha^2}{T} \tag{94}$$

using the τ_α given by Eq. (91). Since such an event could occur over a range of times of order T and the number of sites in the original avalanche is of order T, the total number of primary extra triggers caused by the pulses is of order

$$N_1\sim\alpha^2 T. \tag{95}$$

The spatial density of the primary extra triggers is small so that each of them will cause roughly independent secondary avalanches under the dynamics without further stress pulses. The probability of large avalanches falls off slowly with their size up to the correlation length ξ, which we assume is bigger than T so that the original avalanche was not exponentially unlikely. This means that the total number of jumps in these secondary avalanches will be dominated by the largest one which has size

$$l_{\max}\sim(N_1)^{1/\kappa}. \tag{96}$$

Then the total number of secondary jumps caused by the primary extra triggers is

$$M_2\sim(\alpha^2 T)^{(1+\zeta)/\zeta} \tag{97}$$

using $\kappa=\zeta$.

Each of these secondary jumps has the potential of triggering more jumps due to pulses. The number of such secondary triggers N_2 will be much less than N_1 unless $M_2\sim M_1$; the original number of jumps. Thus, for fixed T, small enough α will cause a small number of secondary jumps, fewer tertiary ones, even fewer quaternary ones, etc. But if

$$M_2\sim M_1\sim T^{1+\zeta}, \tag{98}$$

i.e., $T\sim\alpha^{-2/(1-\zeta)}$, the process will run away. Thus we expect that the stress pulses will become important when

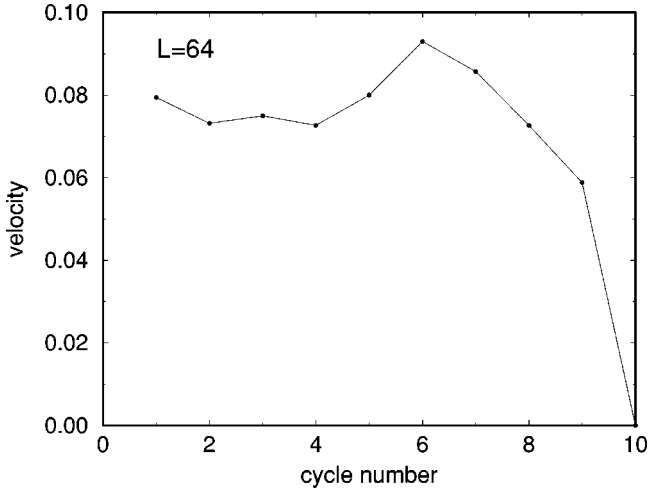

FIG. 18. The velocity of the crack front for the stress pulse model with $\alpha=0.5$, $\gamma=1.5$ is shown as a function of cycle number for a system of size 64 and extent 16 with periodic boundary conditions in the direction of motion. The crack front goes through the same random sample in each cycle and the velocity averaged over each cycle is measured while the external load is kept fixed.

$$\xi\sim\xi_\alpha\sim\alpha^{-2/(1-\zeta)}. \tag{99}$$

Using $1/\nu=1-\zeta$, this corresponds to a reduction in the critical load proportional to α^2, i.e., of exactly the form Eq. (90) that provided a good fit to the numerical data.

Longer range pulses can be considered by a generalization of the above argument. It is found that the α^2 dependence is preserved if and only if $\int dz J_p^2(z)<\infty$, with $J_p(z)$ the peak pulse height (as a function of time) at distance z. Our results for $\gamma>1/2$ agree well with the predicted α^2 dependence of the reduction in the critical load. The marginal case $\gamma=1/2$ is similar numerically and we have not explored smaller γ.

For nonmonotonic models, the no-passing rule discussed earlier and in Appendix A, does not apply. Thus, at least for finite systems and for some length of time, moving and stationary solutions can coexist. Indeed for any nonzero α, we expect that for loads in the range $G_c(\alpha,\gamma)<G<G_c^{qs}$, both stationary and moving solutions should coexist and the selection between the two will be determined by the past history. This effect is seen in Fig. 18 in which the velocity of a crack front of length 64, averaged over a cycle, is shown as a function of the number of times it has passed through a sample of extent $W=16$ with periodic boundary conditions in the direction of motion. In monotonic models, convexity implies that at long times we would measure the same velocity in every pass as there is a unique steady state.[10] But with stress pulses, we see that the velocity changes with the cycle, there is no unique moving solution, and after a number of cycles the crack front can suddenly come to a complete halt, as in Fig. 18, thereby directly illustrating the coexistence of moving and stationary solutions. In finite systems with periodic boundary conditions in both directions as we have used, whether all moving states eventually stop or whether they can survive indefinitely is likely to depend both on the sample and on the load. The question of what happens for infinite systems, we return to in the last section.

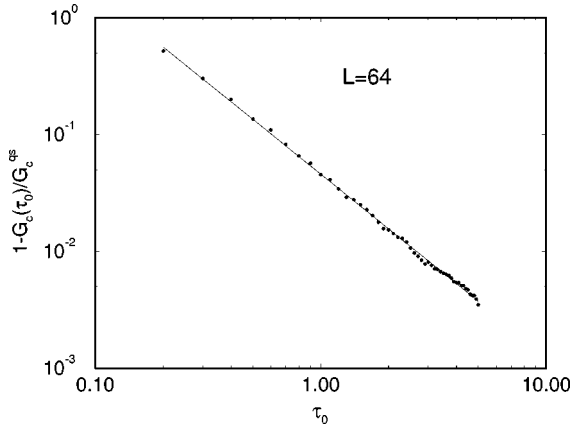

FIG. 19. Log-log plot of the fractional decrease of the threshold force with scalar elastic stress transfer $[G_c^{qs}-G_c(\tau_0)]/G_c^{qs}$ versus τ_0 is shown for systems of size 128. The slope of the linear fit is -1.56.

B. Scalar elastic approximation

We finally consider kernels of the form

$$J_{\rm se}(z,t;\tau)=\frac{(t+\tau_0)\Theta(t-|z|)}{\pi z^2[(t+\tau_0)^2-z^2]^{1/2}}, \tag{100}$$

which is appropriate for the scalar approximation to elasticity. Unlike the sharp pulse models the stress overshoot has a long tail in time. We have cut off the singularity at the sound arrival time by a time τ_0 which crudely represents the microscopic response time. For $\tau_0\to\infty$, this model becomes the monotonic model with the time-delayed kernel.

We measure the threshold load as a function of τ_0, for large τ_0, and find the reduction of the critical load $\langle G_c^{qs}-G_c(\tau_0)\rangle$ is consistent with $\tau_0^{-3/2}$ as shown on a log-log plot in Fig. 19, we do not, however, have an analytical argument for the exponent 3/2. Not surprisingly, we again find that the nonmonotonicity of the kernel is relevant but with a larger eigenvalue that would be expected from the peak pulse heights, presumably because of the long time for which the overshoots are substantial.

C. Velocity and hysteresis

For both the sharp pulse and the scalar elastic models, the stress overshoots lead to velocity versus load curves that are both very noisy and hysteretic. For the scalar elastic case, results are shown for various τ_0 in Fig. 20. As the load is increased, the velocity appears to jump to a nonzero value which is a function of the overshoot's strength and then jump back to zero again on decreasing the load only at smaller load. Thus the stress overshoots *appear* to lead to a first-order-like transition, where the crack front jumps directly to a finite velocity from the pinned phase. Finite-sized systems show hysteretic behavior as shown in Fig. 20. Several cautionary remarks are, however, in order. First, getting statistics on the sizes of hysteresis loops for these nonmonotonic models is numerically intensive. As we saw in Fig. 18, due to the nonmonotonic nature of the models the crack front can come to a complete halt after passing through the system several times. The fluctuations in the mean velocity per cycle

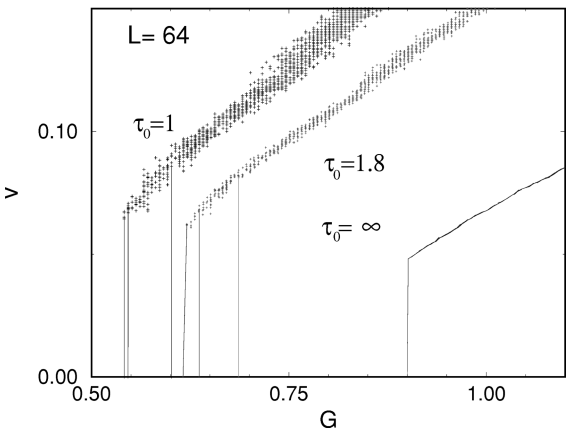

FIG. 20. Mean velocity as a funtion of load for the scalar elastic model, in a single system of size 64, for various values of τ_0 ranging from 1 to ∞; $\tau_0=\infty$ corresponds to the monotonic model with time delays where we expect a continuous transition from the pinned to the moving phase. As can be seen, the finite systems exhibit hysteretic behavior.

of the crack front increases with the size of the stress overshoot but for a given magnitude of the overshoot, decreases as the system size increases. The abrupt stopping of the crack front naturally leads to a large scatter in the size of the hysteresis loops, particularly for smaller systems. Thus, even though the computation time per step increases with system size as $L^2 \ln L$, the scatter in data of the hysteresis loop sizes for small system sizes makes it difficult to study the system size dependence of the hysteresis loops. Second, it is not possible to ascertain whether the crack front will eventually stop or not unless the load is above the $G_{\rm min}^{\rm moving}$ of the quasistatic model, i.e., the largest load at which a static solution exists. Third, it should be noted that the minimum velocities both on increasing and on decreasing the load in Fig. 20 are not all that much bigger than the quasistatic $v_{\rm min}$, even for $\tau_0=1$ for which G_c has decreased by almost a factor of 2. Thus, overall, it is not clear at this point which of the effects that are apparent in the numerics for these nonmonotonic models are finite-size effects and which are indicative of the behavior of much larger systems. We return to this issue at the end of the paper.

V. DISCUSSION

In this last section we compare our results on the dynamics of planar crack fronts with other work and discuss various open questions.

A. Quasistatic limit

In the absence of sound waves, long range-elasticity leads to a nonlocal but monotonic stress transfer kernel in the equation of motion of the front. The transition from the pinned to the moving phase is then second order and there is a unique moving solution above threshold. There are two independent critical exponents in this case and the numerical results we obtain using a discrete model are in good agreement with those from the ε expansion. Note, however that it was necessary to include the effects of corrections to scaling both to get reliable estimates of the exponents and to verify the scaling laws. The dynamic exponent z and the velocity exponent β are both found to be less than one as predicted by the ε expansion. The roughness exponent ζ is very close to the lower bound of $\frac{1}{3}$ which may well be exact, although we have no solid argument for this.

There have recently been two other numerical studies on quasistatic crack models with the appropriate long-range interactions. The first, by Schmittbuhl *et al.*,[22] obtains the same value of the roughness exponent ζ as we do to within error bars. However they obtain a dynamic exponent which is greater than one. It is not clear from their paper as to how this result was obtained and at this point the discrepancy is not understood. The second paper, by Thomas and Paczuski,[23] obtains $\zeta \approx \frac{1}{2}$. Their system sizes are large and it is not at all clear why the results should be so different. One possibility is the dynamical ''updating rules.'' Thomas and Paczuski's are different and more unphysical than ours. Rather than increasing the force adiabatically to depin the most weakly pinned point on the crack front, they depin the point on the crack front that is farthest behind the rest. Whether this or some other difference is the cause of the differences we leave as an unresolved question.

In addition to these numerical studies, there is a very recent experiment[24] in which two halves of a block of plexiglass which have been roughened and then pressure welded together are broken apart. The crack is thus confined to the plane of the original weld. The crack front roughness is measured while it is advancing at a very slow mean speed. With a rather limited range of data, the authors obtain $\zeta=0.55 \pm 0.05$. This would appear to be inconsistent with our quasistatic result, but a systematic curvature appears to be observable in the data and it may be popssible to fit it reasonably well with $\zeta=\frac{1}{3}$ and a $(1/l)^{-1/3}$ correction to scaling (a form with the same number of parameters as an unknown ζ). Another possibility, however, is that the experiments are not really in the quasistatic regime.

These experiments force us to address an issue which we have so far avoided: what determines whether (or in what regime) a crack will behave quasistatically? The basic criterion is *not* directly related to the average velocity of the crack. Rather, it is the speed of propagation of disturbances *along* the crack front—in particular this speed relative to the Rayleigh wave speed c—that is the essential determining feature. But what determines the speed of propagation of disturbances is rather subtle. In general, if the materials that make up the heterogeneous medium are themselves resonably close to ideal elastic solids, then there is no natural parameter which would make the speed of propagation of disturbances along the crack front much slower than c, even if the heterogeneities are weak. But if there is substantial plasticity, creep, or other dissipative effects on the scale of the heterogeneities, then even on these mesoscopic scales the equation of motion of the crack front is *not* given simply by the ''propagator'' Eq. (29) with B its ideal value of order $1/c$. If the system is *velocity toughening* due to these small-scale effects, i.e., the effective fracture toughness on the scale of the heterogeneities increases with velocity—or equivalently that the velocity increases more slowly with load than in an ideal solid—then the linearized dynamics is given by Eq. (29) with a larger value of B. In the limit of very large B, the large-scale behavior of the crack front will

be well approximated by the quasistatic model except very close to the onset of crack propagation where the cumulative effects of the stress pulses caused by a large avalanche will still cause it to run away. Since the exponent z is not much smaller than one, however, the crossover to fully dynamical behavior will occur only very close to the critical load.

Other nonlinear effects—in particular those associated with the local depinning of a section of the crack front caused by the advance of other sections of the crack—will also affect how quasistatic the behavior of the crack front will be. A careful study of several experimental systems—including investigating whether or not the motion appears in bursts of activity when the crack is moving at a slow average speed—would appear to be needed to help resolve this and other related issues.

B. Elastodynamic effects

Close enough to the critical load the quasistatic approximation always breaks down. Since in this approximation the dynamic exponent $z<1$, the effective propagation velocity of the disturbance associated with a quasistatic avalanche of size ξ diverges as ξ^{1-z}, thereby becoming of order the sound speed sufficiently close to the critical load no matter how small the ''bare'' velocity of small-scale disturbances. Thus elastodynamic effects *must* alter the asymptotic critical behavior.

In order to understand the effects of sound-travel time delays, we first considered a simplified causal model in which the dynamic stress transfer is still monotonic. In this model, the static exponents (i.e., ζ and ν) were found to be the same as in the quasistatic approximation because of the monotonic character of the stress transfer. But the dynamic exponent z became equal to one, the minimum value consistent with causality. The scaling identities then imply that $\beta=1$ which is in good agreement with our numerical results on this sound-travel time-delayed model.

But the actual dynamic stress transfer along a crack is more complicated. Indeed, proper inclusion of the dynamics of the medium necessarily leads to a nonmonotonic kernel in the equation of motion of a crack front. In particular, the stress that arises at a point on the crack front due to another section of the crack moving forward, generically rises to a peak before decaying to its long-time quasistatic value.

We have examined the effects of these stress overshoots and find that they are it always relevant at the depinning transition. Specifically, for sufficiently large avalanches the effects of the overshoots build up enough to make such avalanches run away. This causes the crack front to move, at least by some amount, at a load which is *lower* than the quasistatic critical load, i.e., for loads at which there are still stable static configurations. (This can occur because, in the presence of stress overshoots, the ''no-passing'' rule which prevented moving and stationary solutions coexisting in monotonic models is no longer valid.)

If the stress overshoots are weak, their effects will not be important until very close to the quasistatic critical load and there will be a wide regime of validity of the quasistatic results. They will eventually break down only when the correlation length exceeds a crossover length scale which has an inverse power-law dependence on the magnitude of the stress overshoots.

What happens when a large avalanche runs away? We have explored this by numerical studies using simplifed stress transfer kernels which include both sound-travel time delays and stress overshoots. In order to investigate hysteretic effects, we have used finite systems with periodic boundary conditions in the direction of motion with the extent in this direction proportional to the cube root of the length of the crack front, i.e., the scaling of the crack distortions at the quasistatic critical load. In the absence of stress overshoots, moving configurations converge to a unique periodic state. But, due to the nonmonotonicity, this need not be the case once stress overshoots are included.

Nevertheless, for a range of loads between the point $G_{\rm run}$ at which an avalanche runs away and the quasistatic critical load G_c^{qs}, we find that the crack front usually converges to a state which is periodic in time with a period which is some multiple of the time to pass through the system once. If the load is then decreased to below $G_{\rm run}$, the resulting moving state coexists with static configurations which are *stable* to avalanche runaway under small increases in the load. At still lower loads the behavior tends to becomes chaotic, with, in at least some samples, the crack eventually coming to rest only after passing through the sample many times as illustrated in Fig. 18.

The data we have collected thus suggests hysteretic behavior with coexisting moving and stable stationary regimes coexisting in some range of loads from $G_{\rm run}$ down to some lower critical load $G_{\rm stop}$. However, our numerical results indicate that the widths of the hysteresis loops are quite a bit smaller than the difference between the critical load $G_{\rm run}$ and the quasistatic critical load. We would of course like to know whether the hysteretic behavior persists in an infinite system. Unfortunately, the numerics are rather slow in the presence of sound-travel time delays. Thus, obtaining statistics for the sizes of hysteresis loops is numerically intensive and our results are far from conclusive.

C. Possible scenarios near threshold

In this penultimate section we consider various possible scenarios for the behavior of large systems in the presence of stress overshoots. The simplest scenario is suggested by our data: As the loading is increased slowly, the stationary crack jumps to a nonzero velocity at load $G_{\rm move}$, but when the load is decreased, the crack does not stop until a lower critical load $G_{\rm stop}$. At $G_{\rm stop}$ the velocity could either drop to zero discontinuously, presumably the result of an instability of the moving phase, or continuously (as occurs in a hysteretic underdamped Josephson junction). If the load is changed suddenly, this could cause a jump from one phase to the other, perhaps even in the range *above* $G_{\rm move}$ but below G_c^{qs} in which static configurations still exist. Note that the obvious guess, suggested by our numerics, is that $G_{\rm move}=G_{\rm run}$, the point at which avalanches run away and become much bigger than their size in the absence of the stress overshoots. However, it is not obvious that this has to be the case: One could imagine a scenario in which the runaway avalanches eventually stop but only after causing the crack front to become much rougher than it would be under the quasistatic avalanches. A true moving phase might then only exist above a higher load $G_{\rm move}$. This appears rather unlikely and

seems difficult to reconcile with our numerical simulations even though the latter may have been biased by our choice of scaling of the length and the extent of the finite systems.

A second scenario is that, in the limit of large system size, the hysteresis loops we found numerically disappear and the transition becomes ''first order'' with a discontinuous velocity versus load but no hysteresis if one waits a long enough time for the crack to settle down.

Finally, and perhaps most interesting, is the possibility that the onset of crack motion could still be critical with the velocity rising continuously at a critical load and some kind of diverging correlation lengths as the critical load is approached adiabatically from above and from below. This would represent a new universality class of depinning transitions. A variant of this, with the velocity discontinuous but the transition still critical in the sense of diverging correlation lengths, is also conceivable.

Which of the above scenarios obtains may well depend on aspects of the physics that we have left out of our numerical studies and theoretical analysis. For example, multiple scattering of elastic waves from the crack front will cause different regions of the crack front to see stress pulses that depend on the shape of the crack front in their vicinity and that of the segment which has moved. However, we conjecture that the general role of stress overshoots should not be qualitatively changed by multiple scattering since the long-wavelength sound waves will not be strongly affected by the crack roughness unless $\zeta = 1$.

A potentially more important effect is a consequence of vectorial elastodynamics. In particular, for a tensile crack the behavior may be complicated by the fact that the initial stress pulse caused by a section of the crack jumping forwards is *negative* with the stress only becoming positive when the Rayleigh waves arrive. If one hypothesizes a hysteretic velocity-load curve, then in the hysteretic region such a stress transfer kernel can support the coexistence of moving and stationary zones of the crack front with the boundary between the zones moving at a velocity s that corresponds to the zero of the kernel $P(k,\omega)$ (for a Poisson's ratio of $\frac{1}{4}$, $s \approx 0.94c$). In the moving phase, an anomalously tough region could thus cause a stopping ''shock'' to move along the crack front. This might result in a complicated, and very rough, moving state involving large-scale stopping and starting. What roles such shocks might play in the onset of macroscopic crack motion we leave as an interesting avenue for future study.

D. Lattice trapping and nonplanar deformations

In all of our theoretical analysis thus far, we have ignored the effects of lattice periodicity. Indeed, our numerical simulations were specifically set up so as to minimize the effects of periodicity: although our discrete model is periodic in the direction of crack motion, the randomness inherent in Eq. (38), means that it is *statistically* translationally invariant. How will the behavior change in a lattice system with only substitutional randomness?

With quasistatic dynamics, which we consider first, the onset of crack motion will still be continuous but its nature can be quite different. A long perfectly straight crack front will become unstable on increasing the load to a local jump of the weakest segment of one lattice constant. If the randomness is sufficiently weak, even the quasistatic stress transferred by this jump will be sufficient to cause the whole crack to move forward by one lattice constant via the propagation of a pair of kinks nucleated by the first jump. Just above the critical load G_c for a macroscopic motion of the crack, a very long section will need to advance in this manner before a local segment can jump forward by a second lattice constant and cause the process to continue. Thus for loads just above G_c, the behavior will be characterized by straight sections with typical length $\xi(G)$ which diverges as $G \searrow G_c$. This divergence, as well as the form of $v(G)$ will be markedly different from the generic random case discussed in this paper. The behavior will be nonuniversal since it is controlled by the weak-toughness tail of the distribution of the local toughness—in a lattice system simply the bond-breaking energies. This lattice trapping behavior has been studied in a different context by Ji and Robbins.[26]

If the randomness is strong enough, even in a perfect lattice a single local jump is not enough to make the whole crack advance and the behavior near the onset of crack motion should be in the same universality class as that discussed in this paper. Virtually any deviations from a perfect lattice will also cause a crossover to this same randomness-dominated critical behavior. In particular, any small density of random dislocation lines that thread through the plane of the crack with Burger's vectors parallel to the direction of crack advance will destroy the perfect periodicity and prevent the step-by-step advance of the crack from occurring. The segments of the crack front between dislocation lines will act roughly like the segments in our numerical studies and on long scales the behavior will again be that of the random system analyzed here.

The combined effects of elastodynamics and lattice trapping in the absence of randomness have been studied in a two-dimensional model by Marder and Gross.[25] They concluded that $v(G)$ is discontinuous and hysteretic due to runaway caused by dynamic stress overshoots caused by a single jump. The basic effect of dynamic stress overshoots studied by Marder and Gross[25] are qualitatively similar to those we have studied in the three-dimensional random case. Indeed, our *tentative* conclusion is also a discontinuous hysteretic $v(G)$. But even in a perfect lattice, the presence of weak randomness may be enough to bring into play the subtle effects of rare regions discussed in the previous subsection. An understanding of these is, however, well beyond the scope of this paper.

Finally, we have totally ignored all effects of nonplanar crack deformations. These almost certainly play a major role in many experimental situations and may well be important whenever the crack is not confined to a preweakened plane.

ACKNOWLEDGMENTS

We would like to thank O. Narayan, J. R. Rice, and D. Ertaş for useful discussions. This work has been supported in part by the NSF via DMR-9106237, 9630064 and Harvard University's MRSEC.

APPENDIX A

In this appendix we discuss the *no-passing rule*[10] in the context of the quasistatic model and show that the monotonic

model with the time-delayed interactions and the quasistatic models should have the same static exponents. The elastic force in the quasistatic model can be derived from an elastic potential defined as

$$V(\{f\}) = \int dk|k||f(k)|^2, \tag{A1}$$

where k is the wave vector corresponding to the z coordinate and $f(k)$ is the Fourier transform of $f(z)$. This potential is convex in f. Following Ref. 10 consider two configurations of the crack front, $f^G(z,t=0)$ and $f^L(z,t=0)$ with $f^G(z,t=0) \geqslant f^L(z,t=0)\ \forall z$. The no passing rule states that this inequality holds for all times. This can be seen by noticing that if the two configurations were to pass, f^L would have to first approach f^G at some point z. At this point, the random fracture toughness and the external driving force would be identical for both the conformations of the crack front. However, the elastic forces at z on f^L would be less than or equal to that on f^G at z, due to the convexity of the potential. This prevents the passing of f^G by f^L and hence the inequality $f^G(z,t) \geqslant f^L(z,t)$ is obeyed at all times. The no-passing rule also implies a unique moving solution for the crack front in the quasistatic model.[10]

Now consider the monotonic model with the time-delayed interaction. We see that

$$J_{\rm td}(z,t) \leqslant J_{\rm qs}(z,t) \quad \forall (z,t), \tag{A2}$$

where $J_{\rm td}(z,t)$ and $J_{\rm qs}(z,t)$ are the kernels describing the elastic interactions in the two models. This inequality holds when we define the kernel with the sound-travel time-delayed interactions at $z=0$ as in Eq. (81). Thus we see that if we consider two crack fronts, $f_{\rm qs}(z,t)$ obeying the quasistatic equation of motion and $f_{\rm td}(z,t)$ obeying the monotonic time-delayed equation of motion, with $f_{\rm qs}(z,0) = f_{\rm td}(z,0) \forall z$, then following the previous argument we see that $f_{\rm qs}(z,t) \geqslant f_{\rm td}(z,t) \forall (z,t)$. Also since, as $t \to \infty$, $J_{\rm td}(z,t) \to J_{\rm qs}(z) \forall (z)$, we see that, if the load is below threshold, at the end of the avalanche $f_{\rm qs}(z) = f_{\rm td}(z)$. Thus if we start with the same initial configuration, the final positions of the crack front at the end of each avalanche are identical. Thus the static properties are the same for both the models.

By defining the kernels as in Eq. (42), we make sure that both our scalar model as $\tau_0 \to \infty$ and the sharp pulse model with $\alpha = 0$ behave like the monotonic model with the time-delayed interaction.

APPENDIX B

In this appendix we give the explicit forms of the interaction kernels of the various models that we studied numerically.

For the quasistatic approximation, the discretized version of the interaction kernel Eq. (36), with periodic boundary conditions in the direction along the crack front is given, as in Eq. (41), by

$$\tilde{J}_{qs}(z) = \frac{1}{||z||^2} \tag{B1}$$

for $z \neq 0$ and

$$\tilde{J}_{qs}(z=0) = -\sum_{z \neq 0} \tilde{J}_{qs}(z), \tag{B2}$$

where

$$||z|| \equiv \min(|z|, |L-|z||). \tag{B3}$$

In the case of the monotonic model with the time-delayed interactions, the discretized version of the interaction kernel Eq. (37) is given by

$$\tilde{J}_{td}(z,t) = \frac{1}{||z||^2} \Theta(t - ||z||) \tag{B4}$$

for $z \neq 0$. As noted in the text and in the previous appendix, there is an ambiguity in defining the kernel at $z=0$, and in order to preserve the monotonicity properties of the kernel we define

$$\tilde{J}_{td}(z=0,t) = -\sum_{z \neq 0} \tilde{J}_{qs}(z). \tag{B5}$$

The other models we consider in this paper have stress overshoots which decay as the stress pulse moves along the crack front. To include these effects with periodic boundary conditions, we design our kernels such that the stress overshoots disappear smoothly after running through the system once, after which time the kernel equals the quasistatic kernel, $\tilde{J}_{qs}$ at all points in space. Thus, for the sharp pulse model defined by the kernel Eq. (89), we choose the discretized kernel to be

$$\tilde{J}_{sp}(z, t \leqslant L/2) = \frac{1}{||z||^2} \Theta(t - ||z||) + \alpha \frac{\delta(t - ||z||)}{||z||^{\gamma}} e^{-1/(L/2-t)} \tag{B6}$$

and

$$\tilde{J}_{sp}(z, t \geqslant L/2) = \frac{1}{||z||^2} \tag{B7}$$

for $z \neq 0$. There is again an ambiguity as to how one chooses the kernel at $z=0$ and we have defined it to be

$$\tilde{J}_{sp}(z=0,t) = -\max\left[\left| \sum_{z \neq 0} \tilde{J}_{sp}(z,t) \right|, |\tilde{J}_{qs}(z=0)| \right]. \tag{B8}$$

Finally, in the case of the scalar model, the discretized form of the kernel Eq. (35) is chosen once again such that the overshoots vanish after they have run through the system once. Thus,

$$\tilde{J}_{se}(z, t \leqslant L/2) = \frac{t+\tau_0}{||z||^2} \frac{1}{[(t+\tau_0)^2 - ||z||^2 e^{-1/(L/2-t)}]^{1/2}} \tag{B9}$$

and

$$\tilde{J}_{se}(z,t\geqslant L/2)=\frac{1}{||z||^2} \tag{B10}$$

for $z\neq 0$. As for the sharp pulse model, we define

$$\tilde{J}_{se}(z=0,t)=-\max\left[\left|\sum_{z\neq 0}\tilde{J}_{se}(z,t)\right|,|\tilde{J}_{qs}(z=0)|\right]. \tag{B11}$$

*Present address: Institute for Theoretical Physics, University of California, Santa Barbara, CA 93106-4030.

[1] O. Narayan and D. S. Fisher, Phys. Rev. B **48**, 7030 (1993).
[2] T. Natterman, S. Stepanow, L.-H. Tang, and M. Leschom, J. Phys. III (France) **2**, 1483 (1992).
[3] O. Narayan and D. S. Fisher, Phys. Rev. B **46**, 11 520 (1992), and references therein; O. Narayan and A. A. Middleton, *ibid.* **49**, 244 (1994).
[4] D. Ertaş and M. Kardar, Phys. Rev. Lett. **69**, 929 (1992).
[5] P. Bak, C. Tang, and K. Wiesenfeld, Phys. Rev. Lett. **59**, 381 (1987).
[6] H. Gao and J. R. Rice, J. Appl. Mech. **56**, 828 (1989).
[7] P. G. de Gennes, Rev. Mod. Phys. **57**, 827 (1985).
[8] G. Perrin and J. R. Rice, J. Mech. Phys. Solids **42**, 1047 (1994).
[9] Sharad Ramanathan and Daniel S. Fisher, Phys. Rev. Lett. **79**, 877 (1997).
[10] A. A. Middleton, Phys. Rev. Lett. **68**, 670 (1992); R. Mackay (private communication).
[11] L. B. Freund, *Dynamic Fracture Mechanics* (Cambridge University Press, Cambridge, 1990).
[12] Sharad Ramanathan and Daniel S. Fisher (unpublished); Sharad Ramanathan, Ph. D. thesis, Harvard University, 1997.
[13] Sharad Ramanthan, Deniz Ertaş, and Daniel S. Fisher, Phys. Rev. Lett. **79**, 873 (1997); H. Larralde and R. C. Ball, Europhys. Lett. **30**, 287 (1995).
[14] B. Lawn, *Fracture of Brittle Solids*, 2nd ed. (Cambridge University Press, Cambridge, 1993).
[15] Note, however, that in an ideal situation, if $G^{\infty}<\Gamma$ the crack will close. In this case $v=A^{-1}(G^{\infty}/\Gamma)$ is negative and the difference $v[1-A(v)]G^{\infty}$, between the elastic energy absorbed by the material and the energy released by healing goes into kinetic energy.
[16] J. R. Willis and A. B. Movchan, J. Mech. Phys. Solids **43**, 319 (1995).
[17] A. A. Middleton, Ph. D. thesis, Princeton University, 1990; A. A. Middleton and D. S. Fisher, Phys. Rev. Lett. **66**, 92 (1991); (unpublished).
[18] A. B. Harris, J. Phys. C **7**, 1671 (1974).
[19] J. T. Chayes *et al.*, Phys. Rev. Lett. **57**, 2999 (1986).
[20] D. Ertaş and M. Kardar, Phys. Rev. E **49**, R2532 (1994).
[21] O. Narayan (private communication).
[22] J. Schmittbuhl *et al.*, Phys. Rev. Lett. **74**, 1787 (1995).
[23] P. B. Thomas and M. Paczuski, cond-mat/9602023 (unpublished).
[24] J. Schmittbuhl and K. J. Måløy, Phys. Rev. Lett. **78**, 3888 (1997).
[25] M. Marder and S. Gross, J. Mech. Phys. Solids **43**, 1 (1995).
[26] M. Ji and M. O. Robbins, Phys. Rev. B **46**, 14 519 (1992).